Sensitivity alteration of fiber Bragg grating sensors through on-fiber metallic coatings produced by a combined laser-assisted maskless microdeposition and electroless plating process

by

Xixi Zhang

A thesis
presented to the University of Waterloo
in fulfillment of the
thesis requirement for the degree of
Master of Applied Science
in
Mechanical Engineering

Waterloo, Ontario, Canada, 2013

AUTHOR'S DECLARATION

I hereby declare that I am the sole author of this thesis. This is a true copy of the thesis, including any required final revisions, as accepted by my examiners.

I understand that my thesis may be made electronically available to the public.

Xixi Zhang

Abstract

This thesis is concerned with sensitivity alterations of Fiber Bragg Grating (FBG), sensors through additive coatings produced by a combined Laser-Assisted Maskless Micro-deposition (LAMM) and electroless plating process. The coatings can also protect the brittle FBG used in harsh environments.

The thesis encompasses design, fabrication procedures, modeling and comparison of experimental and modeling results to gain insight into the advantages and short-comings of the approach.

Starting with the opto-mechanical modeling, a program is written in MAPLE to analyze the effect of different on-fiber metallic materials and coating thicknesses on the sensitivity of FBGs to temperature and axial force. On the basis of the proper material and thickness, the sensitivity of FBG at different thermal and loading strains are predicted. The optimal theoretical data suggests that if the thickness of the Ni layer is 30–50 μm, maximum temperature sensitivity is achieved.

Some experiments are proposed to test the feasibility of the coated FBG sensors. LAMM is used to coat bare FBGs with a 1-2 μm thick conductive silver layer followed by the electroless nickel plating process to increase layer thickness to a desired level ranging from 1 to 80 μm. Our analytical and experimental results suggest that the temperature sensitivity of the coated FBG with 1 μm Ag and 33 μm Ni is increased almost twice compared to a bare FBG with sensitivity of 0.011 ± 0.001 nm/℃. On the contrary, the force sensitivity is decreased; however, this sensitivity reduction is less than values reported in the literature.

Acknowledgements

I would like to take this opportunity to thank my supervisor Professor Ehsan Toyserkani for his great support, help, advice and encouragement during these two years. He provided me such a precious opportunity to study and explore in the academic area. I also want to express my appreciation to Dr. Hamidreza Alemohammad, for his comments, trouble-shooting help and guidance. I would like to acknowledge my thesis examining committee members, Professor Patricia Nieva and Professor Kyle Daun, for their comments and suggestions.

I hereby acknowledge funding support from the Natural Sciences and Engineering Research Council of Canada (NSERC).

I would like to thank my colleagues and friends at Multi-Scale Additive Manufacturing Laboratory of University of Waterloo: Amir Azhari, Ahmad Basalah, Bradley Cotton, Ehsan Foroozmehr, Thomas Hudson, Teresa King, Joyce Lam, Richard Liang, Negar Rasti, Yaser Shanjani, Mihaela Vlasea, and Steven Tong for their friendship, kindness, help and encouragement. I would also like to thank my friends: Ankur Agrawal, Dunya Ghaffari and Fang Zhang, for their precious friendship.

I would like to express my deepest thankfulness and appreciation to my beloved parents, Wenhua and Xirong, for their great support and encouragement.

Table of Contents

List of Figures

List of Tables

List of Acronyms

FBG – Fiber Bragg gratings

LAMM – Laser-assisted Maskless Microfabrication

SEM – Scanning Electron Microscope

EDAX – Energy Dispersive Analysis by X-Rays Spectroscopy

Nomenclatures

Symbol	Description
α	Coefficient of thermal expansion
λ	wavelength
λ_B	Bragg wavelength
$\Delta\lambda_B$	The shift of Bragg wavelength
ν	Poisson's ration of coating
σ_{zz}, σ_{rr}	Stress components of coating in cylindrical coordinates
Λ	Grating period
C_1	Force sensitivity
C_2	Thermal sensitivity
e_{zz}, e_{rr}	Strain components of coating in cylindrical coordinates
E	Young's modulus
F	Force applied on the fiber
n_{core}	Index of refraction of core
n_{clad}	Index of refraction of cladding
n_{eff}	Effective mode index of refraction
p_{ij}	Elements of Pockel's constant matrix
$[p]$	Pockel's constant
t	Thickness
T	Temperature
ΔT	Temperature shift

Chapter 1

Introduction

In early 1970s, one of the main applications of optical fiber based sensors was endoscopic instruments – medical tools to check the inside of human body. The device is a bundle of spatially arranged optical fibers. When light goes through the object of interest into the endoscope, the device made of optical fibers emanates an image correlated with that object spatially[1]. During the same period, the interest of exploring telecommunication applications of optical fiber sensors attracted many researchers.

In the 21st century, photonics technology has turned into one of the primary research fields. The significant development has made optical fiber sensors widely applicable in a lot of industrial fields, such as aerospace, automotive, nuclear, manufacturing and construction industries. One of the most important applications utilizes its sensing capability, to measure and monitor different kinds of parameters such as pH, pressure, displacement, temperature, vibration, force and strain with optical fiber sensors. Unlike some of the other conventional sensors, optical fiber based sensors seem to have more advantages, such as light weight, small size, long-range linearity, high transmission rate capability and robustness to external electromagnetic disturbances [2].

FBG reflector is an important component in the optical fiber based sensors' field. It can be utilized to monitor structural parameters, such as temperature and strain. The gratings are inscribed along the length of the sensor. Temperature or strain variations cause the pitch of grating to vary which results in the shift in reflected wavelength. In other words, the sensors' spectral response is indispensable for analyzing the thermal and strain loads.

Nowadays, FBG is one of the most widely used optical fiber sensors. FBG's outstanding advantages have made a significant improvement to in-situ structural health monitoring. With respect to conventional sensors which can only measure physical parameters on structures' surfaces, FBGs can be embedded inside for structural monitoring. However, there are some limitations in embedding FBG sensors as the sensitivity of the FBG may vary significantly where it is coated with metallic elements required for the embedding process.

To establish a benchmark for the effect of embedding/coating process on the FBG's sensitivity, this thesis was proposed. It will first demonstrate a novel combined laser-assisted technology and electroless plating process to facilitate the embedding process and, second study the FBG sensors' sensitivity due to the produced coating.

1.1 Motivation

The FBG sensors are promising devices with many advantages, and they have attracted many researchers to develop their outstanding sensing properties and their industrial applications. If FBG sensors are embedded into structures, accurate measurement of structural parameters can be obtained for structural health monitoring that is not possible with traditional sensors.

Embedding FBG sensors into low-melting point materials such as plastics is quite simple. But metallic materials are more common and widely used in industrial technologies. Many smart cutting, drilling and welding tools are made of high melting-point metal or alloy, and structural health monitoring is necessary for those structures and tools. However, the process to embed sensors into high melting-point metallic structures is more difficult, because there are some limitations in FBG sensors, such as grating degradation and sensitivity loss in high temperature environment. However, if we embed FBGs within metallic structures, their sensitivity will be

altered. Our group embedded Ni coated FBG into steel and found out that its sensitivity was changed. We also figured out that the metallic surrounding can act as a protective layer enabling FBGs to be used in harsh environment.

This thesis proposes a novel method, using laser-assisted technology and electro-less plating process. LAMM is a direct-writing process and consists of two steps. First one is using silver nano-deposition to coat a thin silver layer on FBG. Then, by using adjusted laser beam, heating and sintering process is applied on the thin silver layer. Electroless plating process is a convenient and inexpensive chemical deposition process. With these two procedures, a bi-material coating is created on the FBG which can not only protect the FBG sensor from being destroyed in harsh environments but also increase the sensor's thermal sensitivity by two times compared with the original bare sensor.

1.2 Short-comings and problems

Embedding FBG sensors into some non-metallic materials, such as concrete, glass fiber reinforce plastics and composite laminates, have been proposed. These embedding procedures do not require high temperature environment, such as inserting the FBG into concrete cylinder with static strain method and modified vacuum infusion process [3-5]. However, when the substrate changes to metal or alloy, these methods are not fit for the process anymore. The embedding procedure needs melting the high melting-point metal or alloy at high temperature, but the UV-written Bragg gratings in optical fibers start to degrade at 250 ℃ and break at higher temperature [6]. To solve this problem, if the brittle FBG sensor is coated with a thin metallic film before high temperature embedding process, then that thin film will protect the sensor from being damaged by high temperature. However, that thin metal film needs to be coated in a low

temperature environment. The most common low melting-point methods to coat thin film in the literature are vacuum brazing, evaporation and ultrasonic consolidation process[7-9]. However, these methods are not flexible for patterning the fibers. For example in vacuum brazing, the result presented that the thin metallic film had dissolved into the brazing alloy and mixed the thin film metal with the metallic structure substrate [7]. Moreover, pressure and temperature controlled chambers are required for monitoring some parameters during the deposition process, which makes the coating process complicated and inconvenient.

Most importantly, the sensitivity of metal coated FBGs is changed due to significant difference of Young's modulus and thermal expansion between Silica and metallic elements. A benchmark that can represent the performance of metal coated FBGs against the coating parameters (e.g., thickness, physical properties) is quite important to future developments of embedded FBGs. A combined process with LAMM and electroless plating has been proposed in the thesis as well.

1.3 Thesis objective and contribution

The objective statement of this thesis is:

Sensitivity Alteration of FBGs thru On-fiber Metallic coatings

To achieve the objective of this thesis, the research was pursued through the following tasks:

1. Developed an opto-mechanical analytical model to simulate thin metallic films coating process,

2. Simulated the model with different kinds of metal coatings and different metallic layer's thicknesses to figure out the optimal material and optimal thickness for coating,
3. Characterized the parameters of LAMM for thin metallic film deposition on FBG sensor,
4. Characterized and coated FBG sensors with bi-material (Ag-Ni) coating layer by LAMM and nickel electroless plating process,
5. Compared the theoretical and experimental results.

1.4 Thesis outline

This thesis includes seven chapters. Chapter 1 describes the motivation of this thesis, some problems and short-comings in the existing methods for thin metallic film deposition and the statement of objective and contributions. Background and literature review of optical fiber sensors, thin metallic film and thin-film deposition process have been detailed in Chapter 2. Opto-mechanical model and simulation analysis are proposed in Chapter 3, and the theoretical results have been demonstrated by the model. Chapter 4 introduces experimental materials, their characterization and the fabrication method of bi-material coating layers. In this chapter, LAMM process and Nickel electroless plating process have been addressed to protect FBG sensor from high temperature and also improve its sensing capability. Chapter 5 demonstrates the experimental results and the microstructure tests and analysis. Chapter 6 presents the calibration process of FBG sensor's thermal and load sensitivity, and also compares the theoretical results in Chapter 3 with the experimental results in Chapter 5, in order to verify if the experimental results are acceptable. Chapter 7 covers the conclusions and the future work.

Chapter 2

Background and literature review

In this chapter, optical fiber sensors, its fabrication methods and sensing principle will be discussed. The available thin-film fabrication methods for coating FBG are also discussed.

2.1 Fiber Bragg grating

Optical sensors are one of the most important sensing devices in the market today, prompting researchers to enhance their performance and develop new generations of optical fiber-based sensing devices. Optical sensors have been used in a variety of applications such as structural health monitoring, bio-medical sensing, vibration measurement and many more.

Fiber gratings are periodic modulations of the index of refraction in optical fibers that are widely used in sensing physical parameters. Fiber gratings with a short period of ~500 nm are called FBG. The gratings are inscribed in the core of a single-mode optical fiber by UV radiation [10]. FBGs can either be surface mounted for surface parameters monitoring or embedded in structures to monitor internal structural parameters. There are a few laser-based methods that embed optical sensors within metallic structures [11-14]. In the laser-based embedding process, a protective layer must be created around the FBGs using cold processes [15, 16]. Then, in a layer-by-layer manufacturing approach, the rest of the part can be manufactured [17, 18]. The embedding processes can change the sensitivity of FBGs, thus, a deliberate design of metallic coating is needed.

To get a full appreciation of how FBG works, we must turn first to its structure. Fiber gratings are permanent modulations of refractive index in optical fiber. The FBG is a refractive

index's periodic variation in the fiber core which is along the length of the fiber [19], and FBG is known as short period reflection gratings.

Bragg gratings are inscribed in the core along the cylindrical optical fiber. Figure 2-1 shows the schematic of the FBG. The core with inscribed gratings always has dopants such as germanium or tin-germanium to obtain a higher refractive index. This core is surrounded by cladding which is made of fused silica. Λ is the pitch of the periodic variation which is the spatial length measured along the core of the fiber [19].

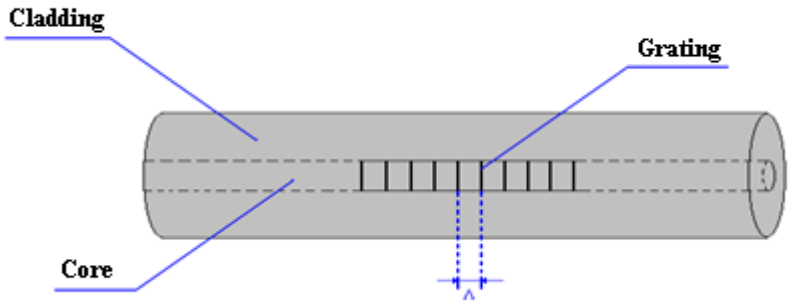

Figure 2-1 Schematic of inscribed gratings in a FBG sensor [10]

Figure 2-2 shows the cross-section of the optical fiber with different refractive index profile. For a single-mode telecommunications fiber, in which the radius of the core is 4 μm, the difference of refractive index from the core to cladding at a wavelength of 1.5 μm is 4.5×10^{-3} [10].

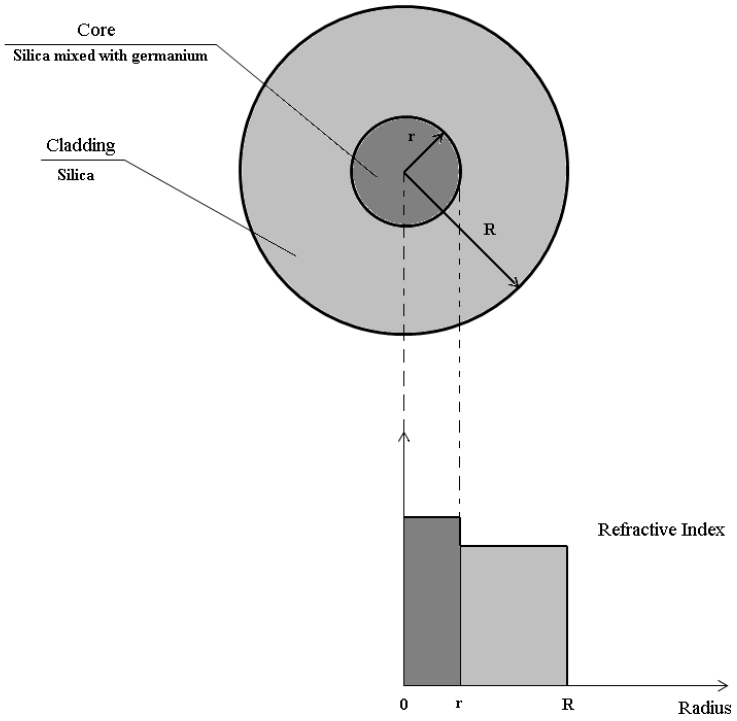

Figure 2-2 Cross-section of optical fiber with its core and cladding corresponding refractive index [10]

When the core of optical fiber is exposed to an intense ultraviolet light, the refractive index will be varied and act as a distributed reflector, which is the principle of FBG. This reflector will filter the backward and forward propagating light beams. The coupling turns the index of refraction increase to high intensity points and results in the specific wavelength called Bragg wavelength (λ_B). As Equation (2.1) shows, Bragg wavelength is a function of the effective propagating mode index refraction and the pitch length of the periodic variation.

$$\lambda_B = 2n_{eff}\,\Lambda \tag{2.1}$$

where λ_B is the Bragg wavelength, n_{eff} is the effective light propagating mode index refraction and Λ is the Bragg grating parameter also known as the pitch length [10, 20].

The FBG can be categorized into different types either by their grating pitch or tilt, for example, the common Bragg reflector, the blazed Bragg grating and chirped Bragg grating. Figure 2-3 shows FBG with different types of grating. The common Bragg reflector has a constant uniform pitch. The blazed Bragg grating has constant pitch, but the grating tilted with respect to the core axis and the angle between the tilted grating and the core axis should be less than 90 °. The pitch of the chirped grating is not uniform and alters along the core axis [20].

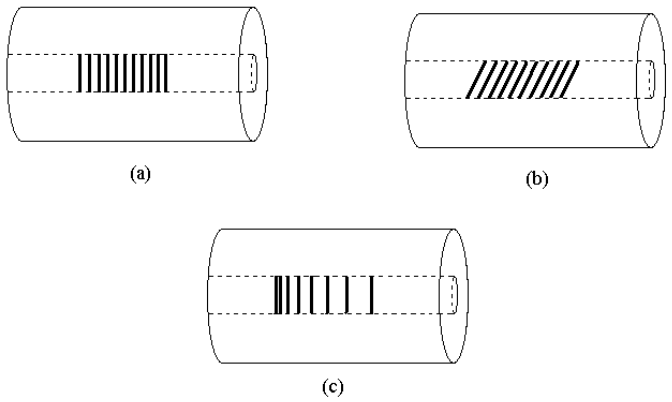

Figure 2-3 Different types of FBG's gratings (a) Common Bragg gratings, (b) Blazed Bragg gratings and (c) Chirped Bragg gratings [20]

2.2 Fabrication method of the FBG

When the optical fiber is exposed to ultraviolet light radiation, the refractive index of this optical fiber is permanently changed. This effect is called photosensitivity [19]. Photosensitivity was discovered by K. O. Hill et al. in 1978 [21, 22], which led to the fabrication techniques of inscribing Bragg gratings in the core of optical fibers. The methods to fabricate Bragg gratings may be categorized into internally written and externally written. However, the internally written

is not that practical, and nowadays, externally written has been widely used in the fabrication techniques.

2.2.1 Internally inscribed Bragg gratings

This internally inscribed technique was discovered by K. O. Hill [21, 22] in 1978. They exposed the core of the photosensitive fiber to argon ion laser, and the fiber was isolated to avoid instability, and laser apparatus was also isolated from heat. In the core, a weak wave intensity pattern would be formed with interference of the laser beam. When the intensity was higher, the index of refraction of the core would be changed permanently. This technique is not that convenient and practical nowadays, but as a historical perspective of the Bragg grating inscription method, this internally inscription is still important to be mentioned.

2.2.2 Externally inscribed Bragg gratings

Based on the internally inscription method, externally inscription technique has been developed.

2.2.2.1 Interferometric inscribing Bragg gratings

The first interferometric inscription approach was proposed by Meltz [23]. In this approach, a UV light laser beam was transmitted through a beam splitter, which split the beam into two parts. The two beams propagated through both amplitude-splitting and wavefront-splitting interferometers. At the end, the two beams were recombined to form an interference pattern which would change the refractive index modulation of a photosensitive fiber core permanently.

Amplitude-splitting and wavefront-splitting interferometers were used in this method. Amplitude-splitting interferometer was used to avoid laser beams low spatial coherence caused by the low quality fringe pattern, and it could vary the two laser beams' intersection angle to inscribe Bragg gratings at any wavelength. However, the sensitivity of the mechanical vibrations could cause gratings to be washed out from the fiber core. So the wavefront-splitting interferometer was used to compensate this disadvantage. With the wavefront-splitting interferometer, only one optical component was required to decrease most of the mechanical vibrations and optimum Bragg gratings could be inscribed. In this interferometric inscribing fabrication process laser sources are also required for inscribing Bragg gratings in interferometric techniques [20, 24].

2.2.2.2 Phase mask technique

Phase mask technique is one of the most efficient ways for writing Bragg gratings. This method applies a phase mask, which is formed holographically, to modulate the UV inscribing beam spatially. The most common UV sources in this technique for gratings fabrication are KrF excimer lasers. The advantage of this method is the greatly simplified gating fabrication system [20, 25].

2.2.2.3 Point-by-point fabrication

The point-by-point technique brings on a shift of the refractive index in the core of optical fiber, one shift at a time. When an excimer laser radiates a focused UV light through an ultra-narrow silt, the refractive index of the core exposed in the radiation part is increased. Then the fiber is translated to Λ distance, and the gratings with the pitch of Λ could be formed by repeating this process. Because the grating is built one point at a time, the Bragg grating's

parameters, such as grating length and pitch, could be changed flexibly. However, this method requires long process time [20, 26].

2.2.2.4 Mask image projection

This process needs a mask projection system, which includes an excimer laser source and a transmission mask. The UV beam is incident from the mask, transmitted through a fused silica high-resolution system and the core of fiber is imaged on the mask. The main advantages of this method are its simplicity of the equipment requirement and the flexibility when compared with other fabrication methods [20, 27].

2.2.2.5 Special fabrication

Processes such as single pulse inscription, long fiber Bragg gratings, chirped gratings and phase-shifted gratings fabrication techniques are categorized as special fabrication [28-31].

2.2.2.6 Summary

Although there are differences in the design, process and equipment in the above grating fabrication methods, one component is the same that the laser has always been used as a radiation source for grating inscription. The externally written technique has now been widely used in grating fabrication processes. The advantages are simplicity, flexibility and proper control.

2.3 Sensing the thermal and the strain exert on the FBG sensors

2.3.1 Principles of sensing with FBG

FBG waveguide is a function of thermal, stress, strain, force and vibration, and the waveguide is also sensitive to the refractive index of the core and cladding. To find out how FBG

is used for monitoring, one parameter X has been involved. This X is assumed as the external parameter. The reflection wavelength of FBG is dependant on X; this X can be thermal strain or loading strain. From Equation (2.1), the Bragg wavelength with parameter X can be calculated as follows [10],

$$\lambda_B = 2n_{eff}\,\Lambda \tag{2.1}$$

$$\frac{\partial \lambda_B}{\partial X} = 2\Lambda\,\frac{\partial n_{eff}}{\partial X} + 2n_{eff}\frac{\partial \Lambda}{\partial X} = 2\Lambda\delta n_{eff} + 2n_{eff}\Lambda\alpha \tag{2.2}$$

$$\frac{1}{\lambda_B}\frac{\partial \lambda_B}{\partial X} = \frac{2\Lambda\delta n_{eff}}{2n_{eff}\Lambda} + \frac{2n_{eff}\Lambda\alpha}{2n_{eff}\Lambda} = \frac{\delta n_{eff}}{n_{eff}} + \alpha \tag{2.3}$$

Combining Equation (2.2) and (2.3),

$$\Delta\lambda_B = \frac{\partial \lambda_B}{\partial X}\Delta X = \lambda_B\left(\frac{\delta n_{eff}}{n_{eff}} + \alpha\right)\Delta X \tag{2.4}$$

where $\frac{\delta n_{eff}}{n_{eff}}$ is the sensitivity of the effective mode index, and α is the coefficient of the Λ length shift which is depended on X. Take for instance temperature change. If we change X to T, the refractive index changes to $(\frac{1}{n_{eff}})(\frac{\partial n_{eff}}{\partial T})$, and α turns out to be the thermal expansion coefficient [10].

2.3.2 Temperature measurement with FBG

When the temperature is changed, the wavelength changes. From Equation (2.4), $\Delta\lambda_B$ as a function of temperature is

$$\Delta\lambda_B = \lambda_B\left[\left(\frac{1}{n_{eff}}\right)\left(\frac{\partial n_{eff}}{\partial T}\right) + \alpha\right]\Delta T \tag{2.5}$$

where $[(\frac{1}{n_{eff}})(\frac{\partial n_{eff}}{\partial T}) + \alpha]$is also called thermo-optic coefficient [10].

By defining each coefficient, the shift in the Bragg wavelength through thermal expansion can be calculated.

2.3.3 Strain measurement with FBG

Figure 2-4 shows the shifts of the wavelength and the grating pitch length before and after the strain is added on both ends of the fiber. By using those shifts, the change in the strain can be obtained.

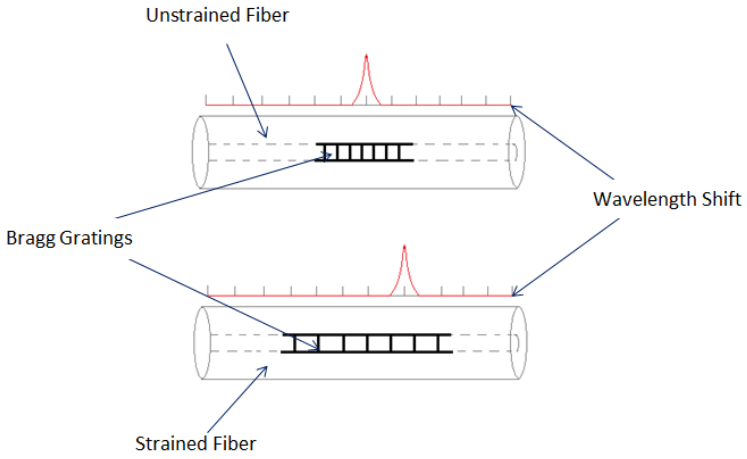

Figure 2-4 Wavelength shift and pitch length shift when strain is added on the FBG [32]

From Equation (2.4), $\Delta\lambda_B$ as a function of strain can be defined as [10]

$$\Delta\boldsymbol{\lambda_B} = \boldsymbol{\lambda_B}(1- \boldsymbol{\rho_a})\varepsilon \tag{2.6}$$

$$\boldsymbol{\rho_a} = \frac{\boldsymbol{n_{eff}^2}}{\boldsymbol{2}} [\boldsymbol{\rho_{12}} - \sigma(\boldsymbol{\rho_{11}} - \boldsymbol{\rho_{12}})] \tag{2.7}$$

where ρ_{11} and ρ_{12} are the stress-optic coefficients and σ is the Poisson's ratio [10].

By defining all coefficients, the shift in the Bragg wavelength through strain expansion can be calculated. The strain sensitivity of that FBG sensor can be obtained from the slope of Equation (2.6).

2.3.4 FBG sensors for structural health monitoring

Many industries, such as the aerospace industry, the automotive industry, and the manufacturing industry, need the real-time and in-situ monitoring for structures' parameters (temperature, strain, and stress). Since the conventional sensors can only detect the parameters on the surface of the structures, a sensor which can be embedded within the structures for internal structural health monitoring is demanding. One of the most common sensors for structural health monitoring is FBG optical sensor. When compared with the other conventional sensors, FBG sensors have more advantages, such as light weight, small size, long-term durability, long-range linearity, and especially the robustness to external electromagnetic fields and disruptions [2].

There are many papers in literature that have discussed how to embed the FBG sensors into the non-metallic composites. However, few of them have reported about embedding FBG sensors within metallic structures because of the high temperature process requirement. It is necessary to melt the high melting-point metal during the embedding FBG sensors with the metallic structures process. The FBG sensor is a highly sensitive optical sensor; it is made of silica and cannot keep its sensitivity in high temperature environment without being damaged. Many questions are associated with embedding FBG into metallic structures. The significant one is that the highly delicate FBGs would be damaged during high temperature embedding process, since the UV-written gratings in the core of optical fiber start to degrade at around 250℃ and

break at higher temperatures [6]. As a result, FBG sensors cannot be embedded in metallic materials using high temperature processes. To solve this problem, a low temperature process is needed. One low-melting-point process is depositing thin metallic film on the bare FBG sensor first, and then manufacturing the FBG with other process to increase the thickness of the thin metallic film.

2.4 Thin metallic films on FBG sensors

As mentioned previously, the thin metallic films can be a useful method to protect the FBG sensor from high temperature damage. Thin metallic films can be made of any kind of metallic materials. When considering the Young's modulus, Poisson ratio and thermal expansion coefficient, the metallic material that fits for FBG sensor coating can be determined. In some studies, bi-material film has also been applied. The bi-material film could both protect FBG sensors from high temperature damage and improve the sensitivity of FBG sensors. The first layer of bi-material films coating is always thin, the thickness of which is 1 μm to 2 μm, and this layer is always used as a conductive layer. Then, on the first thin conductive film, another thicker metallic film is deposited. The second film is always used for high temperature protection and sensitivity improvement. Thicker the second film is, higher is the thermal sensitivity of FBG. However, it will lead to lower force sensitivity. Compared with silica, metal has higher coefficient of thermal expansion. When the environment temperature increases, the metallic coating expands more than silica which results in the pitch length (Λ) elongating more than that of the silica fiber without metallic coating, which makes coated fiber's thermal sensitivity higher. On the contrary, when force is applied on the fiber, the coating will prevent the fiber being strained. This will make the pitch length extend less than the fiber without metallic coating, which makes the force sensitivity reduced.

2.5 Thin metallic film deposition processes

Low-melting-point processes such as electroplating, vacuum brazing method, evaporation, ultrasonic consolidation process and electroless plating process have been applied to deposit metallic coating on the bare FBG sensor recently [7, 9, 18, 33, 34, 35] .

Sandlin et al. [18] developed a coating method with electroplating process. They used Tollen's silver mirror test to coat optical fibers with silver. The coating material was made by the reduction of silver ammonium complex with glucose. With the conductive silver layer, they applied the electroplating method to deposit a nickel layer for further embedding process. Sandlin et al. [7] also reported on placing the metal coated FBGs sensor in a groove of Inconel and covering the groove and FBG by using a vacuum brazing method at 1050 ℃. The metallic coating FBG in Inconel was tested at high temperature and can be stable for a long time. However, if vacuum brazing coated the bare fiber directly with the brazing alloy, then the brazing alloy would not contact with the fiber tight enough and the surface of the fiber would be etched resulting in a joint with Inconel. Iadicicco et al. [9] coated optical fiber sensors with a gold layer at nano-scale with evaporation process. However, the sensitivity of the embedded sensor has not been reported in any of these studies.

Li et al. [33] used a low temperature process of magnetron sputtering to coat FBGs with a titanium film ~1 μm thick followed by ~2 μm thick nickel film over the titanium film. They then used electroplating to plate a protective nickel layer with a thickness of 0.5-1 mm. With the protection layer, their FBG sensors could be safely embedded into metals with a high temperature process such as laser fusion or a casting process. This method is very successful; the thermal sensitivity of their FBG sensor is two times higher with the respect to the original bare FBG. However, this method has one problem with the residual stress which may affect the strain

sensitivity. Feng et al. [34] studied the temperature sensitivity of FBGs coated with copper and nickel. The method of coating process is combined by electroless and electroplating processes. They found out that coated FBG with Cu-Ni, Cu, Ni-Cu and Ni showed different thermal sensitivity. They compared those coating materials and tested their thermal sensitivity coefficient. The sensitivity result showed that: Cu-Ni > Cu > Ni-Cu ≈ Ni, where the Cu-Ni coating is the optimum. However, they also reported that the oxidization of the copper in the air would change the sensor's performance. They suggested that the optimum coating material in their application was Ni-Cu. Mou et al. [35] utilized ultrasonic consolidation process (UC) to embed FBG sensors within aluminium alloy. With the Al coating, the FBG sensor can be used to test responses of temperature, loading, and bending with higher sensitivity. Li et al. [13] prepared three FBG sensors: sample 1 was a bare FBG, sample 2 was a Ni coating FBG fabricated with Ni chemical plating process and sample 3 was a Ni coating FBG manufactured by chemical-electro plating process. Those three samples were embedded in alloy by ultrasonic welding process, and only the sample 3 worked properly with the enhancement of thermal sensitivity.

The bi-material film is always used for high temperature protection. The sensitivity of FBGs plays an important role in the performance and industrial acceptance of such sensors. The sensitivity required for FBGs is highly dependent on applications, environment of use and the magnitude of physical parameters measured by the sensors. In addition, such sensitivity dependency is more complicated if FBGs are embedded in metallic structures using laser-assisted additive coating processes. In summary, the coating not only acts as a protective layer but also alters the sensor sensitivity. Therefore, the coating process should not create high temperature on the sensors as FBGs' gratings are degraded at high temperatures, consequently the sensors functionality will be jeopardized. The UV-written gratings in optical fibers start to

degrade at around 250℃ and break at higher temperatures [6]. After finding out methods to protect the optical sensor from high temperature during the embedding process, the next step is trying to obtain higher sensitivity of the optical sensor to improve its sensing capability.

Lupi et al. [36] reported the enhancement of the sensitivity of FBG sensors at cryogenic temperature by coating the FBGs with thin films of various metals such as tin, lead, zinc and aluminum, by the method of casting and electrocoating processes. The sensitivity of FBG was measured at cryogenic temperature, and lead coated FBG showed the highest sensitivity. They also found out that zinc coated FBG sensor did not work well below 15K. Feng et al. [37] described an etchless duplex metal coating to enhance the FBG's temperature sensitivity, and found that Ni-Cu coated FBG sensor has both higher temperature repeatability and higher thermal sensitivity. The sensitivity of the FBG coated with Ni-Cu layer was reported to be 0.01886nm/℃. The boundaries of FBG surface, copper layer and nickel layer are all clear, without any joint in them, the performance of this bi-material film showed very good quality. Lee et al. [38] developed an FBG sensor encapsulated into cylindrical copper/ceramic tube, and figured out that the thermal strain of these two materials can help to improve FBG's thermal sensitivity. The thermal sensitivity for copper tube and ceramic tube are 0.033nm/℃ and 0.028nm/℃ respectively. They suggested using higher thermal expansion coefficient material as tube material to increase FBG's thermal sensitivity. Song et al. [39] improved the FBG's pressure sensitivity by putting the FBG sensor into a metal package, which is made of Ti-5Al-2.5Sn alloy, and bonded the package's ends with aluminum cylinders.

2.6 Laser-assisted thin-film technology

There are three fundamental groups of processes of thin film laser-assisted technology. The first one is the thin film deposition, second one is the laser patterning process of thin film and the last one is the elemental parameters tuning [40]. The laser-assisted technology used in this thesis is Maskless Microfabrication technology. This technology belongs to laser patterning, which is a laser-assisted maskless method for the surface of a solid structuring directly. This laser-assisted patterning consists of two stages. In the first stage, the nano-particles are formed as a thin-film layer on the substrate surface. Then, in the second stage, a laser-assisted process will be used to make the thin-film sintered on substrate stable [40].

2.7 Fiber optic smart structures

There are three basic functions of fiber optic smart structure system: first is the capability to sense environmental conditions inside, around or on the surface of the structures, second is transmitting the signal back to electronic processor, and the third is that when the information is received by processor, an action will be executed [41].

Fiber optical sensors have a lot of advantages when applied to smart structures. Most common are its small size and light weight. They keep the structures' integrity when optical sensor is embedded into smart structures. Then, since fiber is made of dielectric glass, this material can eliminate the conductive path, and reduce the hazards of internal electrical discharges. Another important advantage is the multiplex functions of the optic fiber, one fiber can monitor different kinds of parameters at the same time [41, 42].

There are numbers of applications of fiber optic smart structures in industrial field nowadays. In the aerospace field, launch vehicle is an example. Optic fibers are embedded in the

tank, rocket nozzles and rocket booster for health monitoring during the manufacturing process[41, 43]. Medical and biological industry also employs optic fiber smart structures. Unlike aerospace industry, medical and biological industries utilize fiber's electromagnetic resistance property to reduce the hazards of electrical shock with dielectric materials [41]. Fiber optic smart structures have also been utilized for earthquakes detection, volcanoes' flow detection and the hazardous of waste materials in containers [44].

2.8 Applications of FBG sensors

The most common application of coated FBG sensors is structural health monitoring. Many researchers have studied this field. Nguyen et al. [45] designed an interrogation system, based on optical FBG sensor, for health monitoring. This system was used to detect acoustic emission on both metal and composite. This novel technique was able to detect strains at high frequency (ultrasonic frequencies for instance). FBG sensor has also been applied in many other fields. Suresh et al. [46] have utilized FBG's shear force sensing capability to develop an FBG sensor for civil structural components monitoring. They embedded the developed FBG sensor in concrete beam and measured contact force at the end of each concrete beam successfully. In another experiment, they also measured the thermal shear stress by the developed FBG sensor. Richter-Trummer et al. [47] reported their FBG measured industrial process approach completely. They mentioned their selection, calibration and the welding process. FBG sensor in their paper was able to record transient and residual strain during the friction stir welding process.

Wu et al. [48] studied the application of long term health monitoring based on FBG strain sensing capability, and found out that the durability of FBG sensor was stable even if the

performance of the material was varied. Amano et al. [49] embedded multiple FBG sensors in advanced grid structure (AGS) to monitor the existent fractures and mechanical strains. Yue et al. [50] presented different types of FBG sensors embedded for an old bridge's long term structural maintenance monitoring. Chong et al. [51] designed a perfect thermal resistance Cu-C coated FBG sensor net to monitor a nuclear power plant at high temperature, and the Cu-C coated FBG sensor could easily detect acoustic ultrasonic waves radiated from laser. Huang et al. [52] proposed an advanced FBG sensor to measure underwater acoustic. First, they transferred the acoustic pressure (its frequency ranged from 2.5 kHz to 12 kHz) to elastic vibration of a circular metal. Then, the vibration would cause modulation of the reflected light wave's intensity. Finally, the light wave would be converted to electric signal, and as a result, the underwater acoustic was measured by FBG.

2.9 Summary

The embedding process of FBG within metallic structures for structural health monitoring is not mature enough. Development of the industrial technologies, improved manufacturing procedures and advanced sensors are required nowadays.

No benchmark for representing the performance of metal coated FBGs against the coating parameters has been mentioned in the literature. The combined LAMM and electroless plating process approach has not been proposed in the literature either. Because of the short-comings of the protective layer deposition approach, a convenient, low-cost and advanced method to coat metallic layer on FBG is required.

Chapter 3

Analytical model

In order to predict the optimum material for FBG's coating, an opto-mechanical model has been developed to analyze the coating's material.

3.1 Opto-mechanical model

The opto-mechanical model predicts the Bragg wavelength shift as a function of temperature and axial force at different thicknesses. The components of axial strain ε_{zz}, and radial strain ε_{rr} in an FBG exposed to temperature and axial force were obtained by using an analytical model developed in Maple software [53]. These parameters were then fed into the opto-mechanical MAPLE model to find the relation between the Bragg wavelength changes ($\Delta\lambda_B$), temperature variations (ΔT) and the strain components. The shift of Bragg wavelength ($\Delta\lambda_B$) in the FBG sensor exposed to loading strain and thermal strain variation was obtained from [53].

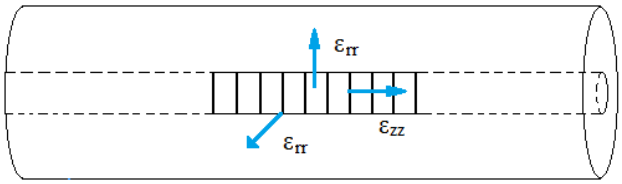

Figure 3-1 FBG subjected to strain field with three strain components

If we assume that FBG sensor is dependent on the temperature change ΔT and strain tensors e_1, e_2 and e_3, where e_1 is along the direction of the grating, as ε_{zz} shown in Figure 3-1 and e_2 and e_3 are the equal transverse strain as ε_{rr} shown in Figure 3-1.

Rewriting Equation (2.4),

$$\Delta\lambda_B = 2(\Lambda\Delta n_{eff} + n_{eff}\,\Delta\Lambda)_{\Delta T=0} + 2(\Lambda\Delta n_{eff} + n_{eff}\,\Delta\Lambda)_{\varepsilon=0} \quad (3.1)$$

then the Bragg wavelength change is

$$\frac{\Delta\lambda_B}{\lambda_B} = \varepsilon_{zz} - \frac{n_{eff}^2}{2}\left[(p_{11} + p_{12})\,\varepsilon_{rr} + p_{12}\cdot\varepsilon_{zz}\right] + \frac{1}{n_{eff}}\cdot\left(\frac{\partial n}{\partial T}\right)\Delta T + \frac{n_{eff}^2}{2}\cdot(p_{11} + 2p_{12})\cdot\alpha\Delta T \quad (3.2)$$

where n_{eff} is the effective refractive index, p_{ij} are elements of Pockel's constant matrix, $[p]$ is Pockel's constant for the photo-elastic effect in optical fibers, also called strain optic tensor, $\frac{\partial n}{\partial T}$ a constant showing the temperature sensitivity of refractive index, α is the coefficient of thermal expansion, and Λ is the grating pitch[10, 53, 54, 55].

$[p]$ is described as [53,56],

$$[p] = \begin{bmatrix} p_{11} & p_{12} & p_{12} & 0 & 0 & 0 \\ p_{12} & p_{11} & p_{12} & 0 & 0 & 0 \\ p_{12} & p_{12} & p_{11} & 0 & 0 & 0 \\ 0 & 0 & 0 & \frac{(p_{11}-p_{12})}{2} & 0 & 0 \\ 0 & 0 & 0 & 0 & \frac{(p_{11}-p_{12})}{2} & 0 \\ 0 & 0 & 0 & 0 & 0 & \frac{(p_{11}-p_{12})}{2} \end{bmatrix} \quad (3.3)$$

According to the FBG Equation (2.1), the Bragg wavelength (λ_B) can be replaced by the term $2n_{eff}\Lambda$, Equation (3.2) can be simplified as

$$\Delta\lambda_B = 2n_{eff}\Lambda\cdot\varepsilon_{zz} - \frac{n_{eff}^2}{2}\left[(p_{11} + p_{12})\,\varepsilon_{rr} + p_{12}\cdot\varepsilon_{zz}\right]\cdot 2n_{eff}\Lambda + \frac{1}{n_{eff}}\cdot\left(\frac{\partial n}{\partial T}\right)\Delta T\cdot 2n_{eff}\Lambda + \frac{n_{eff}^2}{2}\cdot(p_{11} + 2p_{12})\cdot\alpha\Delta T\cdot 2n_{eff}\Lambda \quad (3.4)$$

The values of parameters used in the model are listed in Table 3-1.

Table 3-1 Constant for modeling [53]

Parameter	Value
n_{eff}	1.44405
p_{11}	0.113
p_{12}	0.252
Λ (nm)	537
$\partial n/\partial T$	1.2×10^{-5}

After simplifying Equation (3.2), $\Delta\lambda_B$ is only related to ΔT and axial force (F) applied on the optical fiber. Using Equation (3.4) the sensitivity of the Bragg wavelength to the applied axial force and temperature is obtained.

Further information in modeling procedure can be found in [53] and [56]. In conclusion, the following parameters and assumptions are materialized in this modeling.

1. The values of optical parameters applied in the model are listed in Table 3-1[53].
2. The thermo-mechanical properties of materials used in the modeling to express loading and thermal strain/stress terms are listed in Table 3-1, where E is the Young's modulus, ν Poisson ratio and α is the coefficient of thermal expansion. It should be noted that we used bulk properties in this study as the elastic moduli of thin film should not vary substantially from bulk where dimensions are in micro-scale [57]. The reason is the fact that this property is related to atom-to-atom bonds. For dimensional features larger than nanometer, where the effect of atomic surface

contact is not dominant, it is reasonably correct to consider the bulk properties for thin films [57].

3. By assuming that ΔT is zero, the function of sensitivity and the applied F can be found. Similarly, by assuming that F is zero, the relation between sensitivity and ΔT can also be obtained.
4. The effect of Ag thin film is ignored; therefore, a single material system is considered as the coating in the modeling. As we will discuss later, the bi-material coating includes a thin film of Ag with thickness of 1 μm; however, the inclusion of this thin film along with the other material in the modeling domain imposes convergence problems mainly due to finite precision of computations involving floating point at interfaces in such a discrete and small size system. A study is underway to identify a solution for this numerical issue. If resolved, we will address our methodology in our future article.

3.2 Simulation analysis

By using Maple software, we developed an analytical model, in which temperature and force can be applied on fiber. We obtained the components of axial strain along the fiber direction ε_{zz}, and radial strain ε_{rr}. These parameters are then substituted into the opto-mechanical model to find the relation between the Bragg wavelength changes ($\Delta\lambda_B/\lambda_B$) and the strain components (ε) or temperature variations (ΔT). The shift of Bragg wavelength ($\Delta\lambda_B$) when the FBG sensor is exposed to strain and temperature variations can be obtained from Equation (3.2).

Based on the Bragg wavelength change ($\Delta\lambda_B/\lambda_B$), the sensitivity of the sensor can be obtained. After substituting those parameters and constants into the equation, $\Delta\lambda_B$ is only related to the force applied on the fiber (F) and the temperature shift (ΔT).

$$\Delta\lambda_B = C_1 F + C_2 \Delta T \tag{3.5}$$

where C_1 is the force sensitivity and C_2 is the thermal sensitivity, which are determined by fiber's properties and coating materials' properties and thickness.

By using this model, we can apply different kinds of coating materials on the fibers, compare their characteristics, such as sensitivity, price and manufacturability, to find out the optimum material. After confirming the optimum material, we try to find the optimum thickness of that coating material. Since the higher temperature sensitivity will induce lower force sensitivity, a proper coating thickness which would satisfy the real application is required.

In this thesis, to find the optimum material and thickness, seven materials (silver, nickel, gold, magnesium, chromium, titanium and aluminum) have been used in the model where their thickness varies in the range of 1 to 1000 μm. Based on the model, both thermal and force sensitivity will be kept as a constant approximately after 100μm. The following theoretical data just shows the variation of result in the range of 1 to 100 μm.

To prove the reliability of this model, Alemohammad has proposed the uncertainty of this model and the comparison of results in [56]. Comparing the result from the model of bare sensor with the experimental results, when Bragg wavelength is measured as a function of temperature, the temperature measurement error is ±0.56 ℃, and the Bragg wavelength measurement error is ±5pm. The difference in thermal sensitivity between the model and experimental result is 0.9%. For the axial force, the Bragg wavelength error is also ±5pm, and the force measurement error is

0.88mN between model result and experimental result. The force sensitivity difference is 7%. Based on the difference in both thermal and force sensitivity, the model results are acceptable.

3.3 Theoretical results

The model was run for seven single material coatings with silver, nickel, gold, magnesium, chromium, titanium and aluminium with the thickness in the range of 1 to 1000 μm.

The properties of the materials are shown in Table 3-2. In the table, E is the Young's modulus, Poisson ratio is shown as ν and α is the coefficient of thermal expansion. According to the model, the sensitivity depends on these three parameters. All these three parameters need to be considered when choosing the material. Material with a lower Young's modulus, higher Poisson ratio and proper coefficient of thermal expansion will be a better choice.

Table 3-2 Properties of the materials [58]

	Silica	Ag	Al	Au	Cr	Ni	Ti	Mg
E(GPa)	75	83	70	79	279	200	116	45
ν	0.17	0.37	0.35	0.44	0.21	0.31	0.32	0.29
α(μm/m*K)	0.55	18.9	23.1	14.2	4.9	13.4	8.6	24.8

The reason we chose these seven materials is that we tried to select different E, ν and α from the minimum value to the maximum value, which can cover most of the metallic materials.

Figure 3-2 represents a relation between the temperature sensitivity and the coating thickness. Figure 3-3 shows the axial force sensitivity versus the coating thickness. A glance at the plots reveals that the coating reduces force sensitivity whereas it increases the temperature

sensitivity. The increase in the temperature sensitivity stems from the higher thermal expansion of metallic coating compared to the optical fiber.

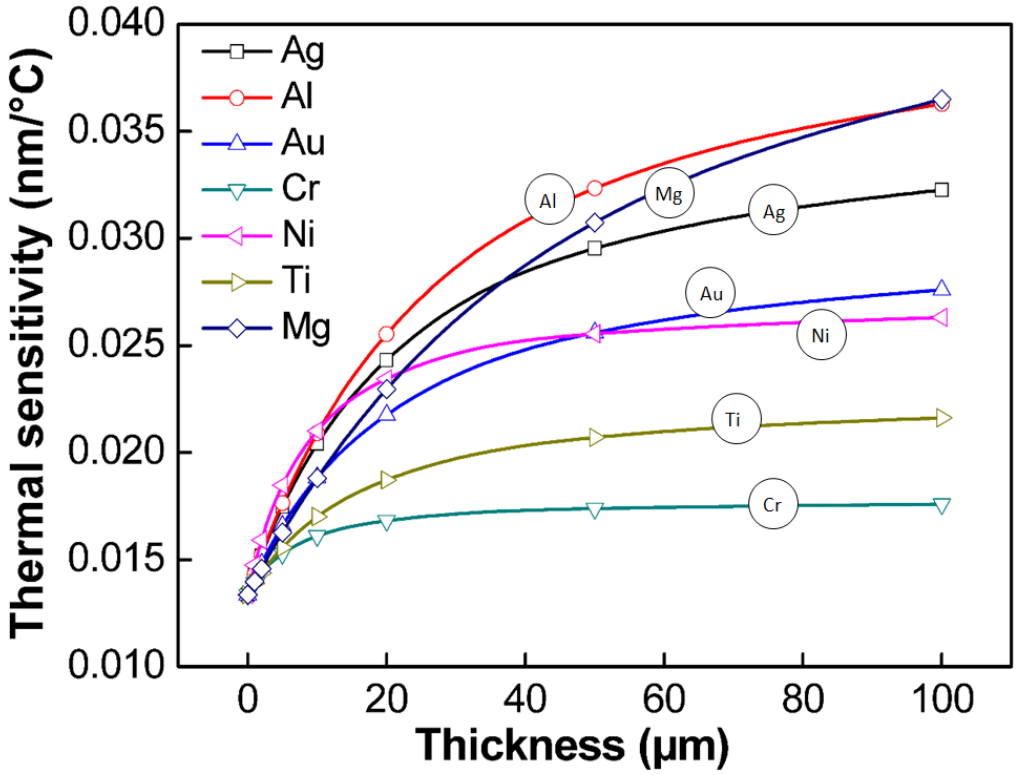

Figure 3-2 FBG's temperature sensitivity versus the coating thickness with different materials

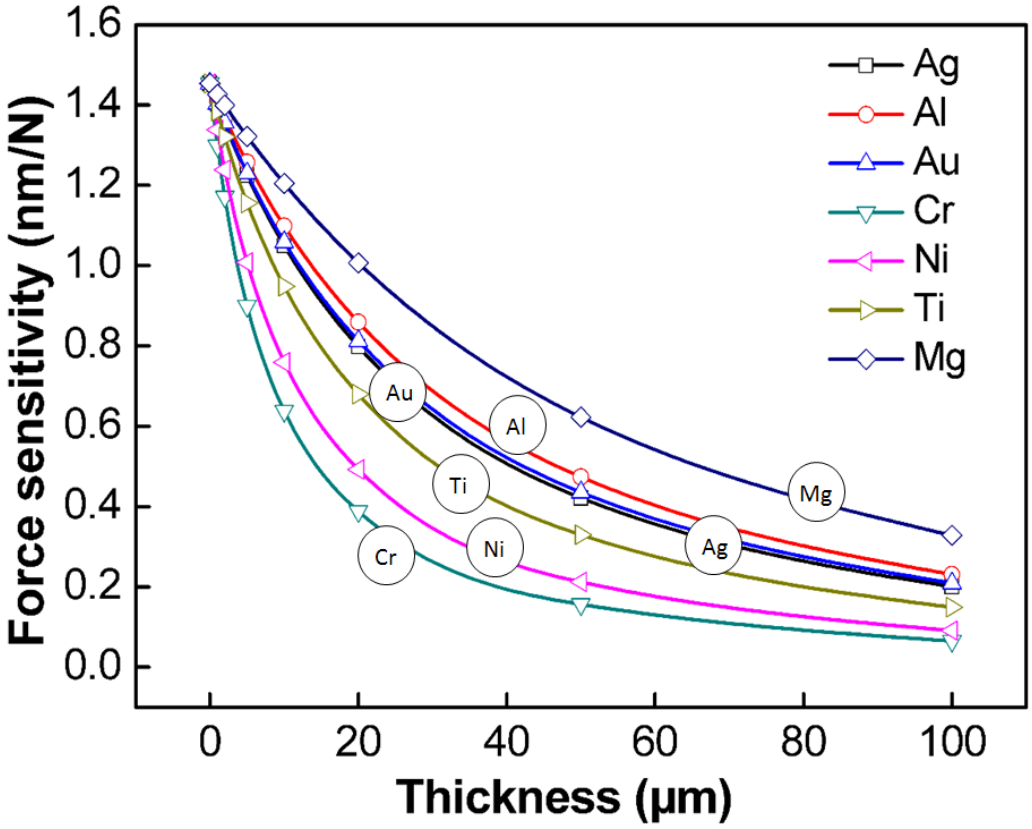

Figure 3-3 FBG's force sensitivity versus the coating thickness with different materials

Based on the analytical model, we narrowed down the variation range from 1 to 100 μm, and combined curves to produce Figure 3-2 and Figure 3-3. As seen in Figure 3-2, silver, magnesium, aluminium, gold and nickel exhibit higher sensitivity for temperature. After thickness is increased to 40 μm, except Mg and Al (which will be discussed later), others coatings' thermal sensitivity has shown to be constant for most of these seven materials. The increment in thermal sensitivity for increasing coating thickness from 40 μm to 100 μm is less than 0.002nm/℃ which is not worthy. To decrease the material cost, we select the coating thickness less than 40 μm.

When comparing the coefficient of thermal expansion, metallic coatings' are much higher than silica's. When the temperature is changed, the metallic coating will expand more than silica, which will result in gratings shift more than that without coatings. Λ is the original FBG's pitch length at T. We assumed that Λ_1 is the FBG's new pitch length at T_1 and Λ_2 is coated FBG's pitch length at T_2. Λ_1 is less than Λ_2, and Λ is less than both Λ_1 and Λ_2. Based on Equation (2.1), (3.4) and (3.5), when Λ gets larger, C_2 will get larger. C_2 is the thermal sensitivity, that's why the coating can increase the thermal sensitivity.

Figure 3-3 suggests that the force sensitivity reduction is less for magnesium, aluminium, gold and silver. The force sensitivity also becomes constant after a value. When considering higher thermal sensitivity and less reduction of force sensitivity, we have selected the thickness in the range 30-35 μm. Also, the difference from 40 μm to 100 μm is less than 0.1nm/N. To decrease the material cost, we still select the coating thickness less than 40 μm.

The principle of force sensitivity reduction is the similar to the thermal sensitivity enhancement. When the force has been applied on the FBG, the coating will prevent the FBG from expanding as much as the bare FBG does. The coated FBG's pitch length shift will be less than the bare FBG's, resulting in the force sensitivity reduction for the coated FBG.

After we selected the optimum thickness, we needed to determine the optimum material. Although the coating reduces the force sensitivity for all elements, it is less reduced if magnesium or aluminium is produced on the fiber. Although Mg and Al are well suited for sensitivity enhancement, they are not stable enough at room temperature as they are prone to oxidization easily ($2Mg+O_2 \rightarrow 2MgO$ and $4Al + 3O_2 \rightarrow 2Al_2O_3$). In addition, their manufacturability as coatings for optical fibers on micro-scale is one of the significant problems.

According to the analytical analysis, Ag and Ni also exhibit superior effects on temperature sensitivity where Ag has less effect on the force sensitivity reduction. However, Ag is a precious metal; it is too costly if we produce thick Ag layer on FBG. Also, the production process is difficult for thick Ag layer deposition. Ni is much cheaper, Ni electroless plating process is inexpensive, and also a cold process which will not degrade Bragg gratings at all. But Ni electroless plating process needs a conductive layer on fiber. We chose Ag as the thin conductive layer which was produced by direct-writing process, the LAMM process.

Since Ag can be injected by LAMM process and Ni can be electroless plated, these two metals are manufacturable. From the figures above, we chose the bi-material of Ag-Ni for this study. In order to have the maximum enhancement in temperature sensitivity and the minimum reduction in force sensitivity, 1 to 2 μm thickness of Ag layer and 30 to 35 μm thickness of Ni layer was considered as the optimum thickness for our experiments. In addition, the thin Ag seed layer will positively improve temperature sensitivity. This Ag-Ni coating is just one of the optimum conditions and the process is manufacturable and inexpensive.

3.4 Summary

This model is dependent on the coating material's properties, such as: Young's modulus, Poisson ratio and coefficient of thermal expansion, to analyze FBG's thermal and force sensitivity. We have tested seven metallic materials as coating materials and found the one with optimum thickness. The FBG's sensitivity with optimum coating material and optimum thickness has also been predicted in this chapter.

Chapter 4

Experimental materials, characterization and fabrication methods

This chapter discusses materials for experiment and fabrication methods. In this thesis, two fabrication methods have been used. One method is a laser-assisted technology, and the other one is chemical plating process - electroless plating. The experiment is aimed to coat bi-material thin-film layer on FBG for both protection and sensitivity enhancement. The characterization and the process development of each method have also been addressed in this chapter.

4.1 Materials and preparation processes

The bi-material thin-film layer was made of Ag-Ni. The first Ag layer of thickness 1 – 2 μm was deposited by LAMM process. This Ag layer worked as a conductive layer for helping Ni layer deposition. Ni electroless plating was then applied on the thin Ag layer. The desired level of Ni layer thickness should be ranging from 1 to 80 μm. The thickness of the Ni layer depends on the Ni plating bath time. The function of Ni thickness and bathing time was linear. To identify an optimum coating thickness and predict its effect on the sensor sensitivity to force and temperature, an opto-mechanical model was developed. The details of opto-mechanical model have been discussed in chapter 3. According to the model, if the thickness of the Ni layer was 30–35 μm, the optimum sensitivity would be achieved.

4.1.1 FBG preparation

The FBG sensors (written in SMF28, QPS Photronics, Pointe-Claire, QC, Canada) and regular bare fibers were used for trials and experimental studies.

Before the bi-material coating could be deposited on the FBG, some preparation is required. The FBG must be cut to a special length and a portion of the polymer coating should be removed. The procedure is as follows [59]:

1. Cut the fiber

   Cut the fiber to 250mm, with 69mm to the left of the Marker 1. The Bragg gratings are located between Marker 1 and Marker 2. The length of 250mm is to fit the rotator stage which will be applied later in the deposition process.

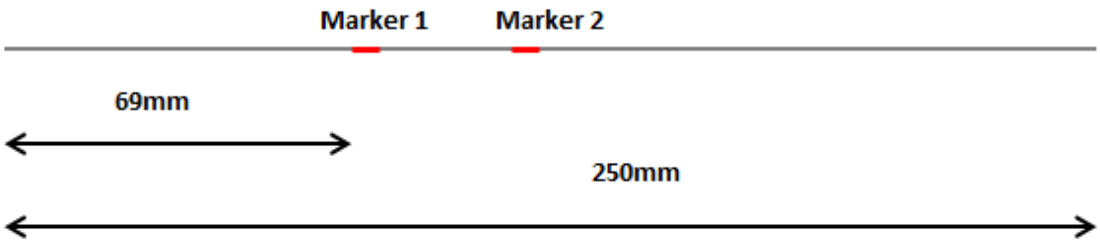

Figure 4-1 The general view of markers on 250mm FBG [59]

2. Strip the fiber

   Since Bragg gratings are located between Marker 1 and Marker 2, to coat Ag directly on gratings, the polymer coating on Bragg gratings must be removed. First the polymer coating was removed by using the Micro-Strip fiber strippers to the left of Marker 1. Since the Bragg gratings are so brittle and located between Marker 1 and Marker 2, from protective consideration, a furniture stripper was used to gently remove the polymer coating to the left of Marker 2.

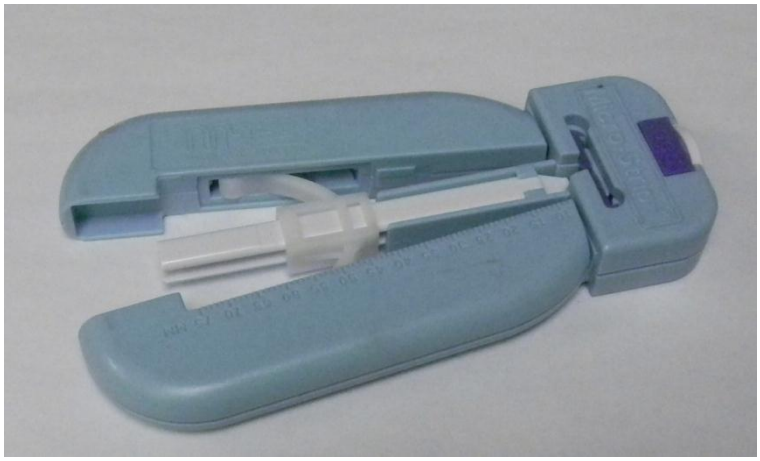

Figure 4-2 Fiber strippers for polymer removal

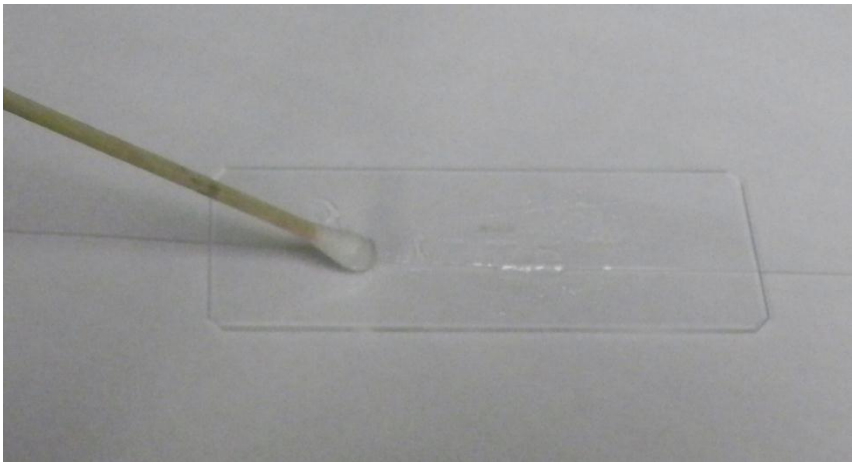

Figure 4-3 Removing polymer with furniture stripper

3. Clean the fiber

   To achieve better quality silver coating, the stripped fiber must be cleaned to remove the polymer fragments. The stripped fibers were cleaned with Kim-wipe™ and acetone, followed by gentle cleaning using isopropanol.

4.1.2 Silver nano-particles

The LAMM system was used for the direct printing of Ag nanoparticles on optical fibers with Ag nano-ink. For thin film deposition, Ag nano-particles (CSD-32, Cabot Corp, Boston,

MA, USA) suspended in ethylene glycol with a weight percentage of 45-55 wt% was used, and the average particle size was less than 60 nm. Thin layer (1-2 μm) of Ag layer was deposited on the bare fiber. Figure 4-4 shows the atomizer reservoir, the silver ink bottle and the atomizer tube. The silver ink bottle was immersed in the deionized water. There were two reasons that silver was chosen for the first conductive layer. Firstly, silver was one of the materials which were available among the nano-inks, and secondly, it has higher thermal expansion when compared with silica. Due to higher thermal expansion, higher thermal sensitivity would be obtained. The analytical model has simulated different metallic materials as the deposition layer and figure out their sensitivity theoretically in the above chapter.

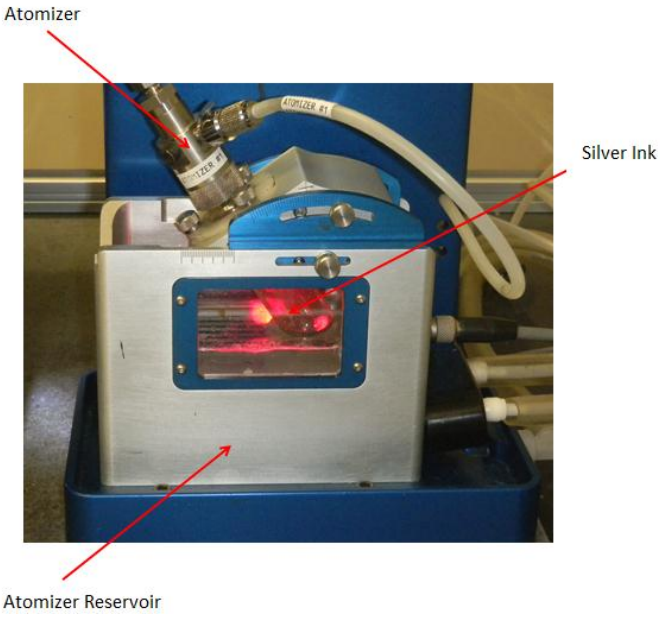

Figure 4-4 Silver ink and Atomizer Reservoir

4.1.3 Ni electroless plating solutions and activation materials

After thin-film Ag layer had been deposited on fiber, the next step was Ni electroless plating. The solution of Ni electroless plating process was from CASWELL, USA. We faced

several problems during the Ni electroless plating process. At first, the solution was set as the introduction manual from the CASWELL mentioned. The first ratio from the introduction book was Water: Part B: Part A = 16:3:1, however, the size of the fiber was too small to deposit in chemical solution, the diluted solution couldn't plate Ni on the Ag layer, and the ratio from introduction was not fit for this research. Then, although we adjusted the solution ratio by increasing the concentration of Ni^{2+}, there was still no deposition on Ag layer. From literature [60, 61], we realized that the plating process needs to be activated by activation materials. Therefore, in this experiment, two kinds of activation materials were used. One was 5% $PdCl_2$ solution from ArtChemicals Company, and the other was a piece of steel. By immersing the fiber with Ag coating in 5% $PdCl_2$ solution, an extremely thin layer of Pd^{2+} would form on Ag layer which would lower the reaction barrier of Ni deposition. After this procedure, the fiber was cleaned in deionized water. During the Ni electroless plating process, the fiber also needed to be placed on a piece of steel to activate the reaction. By using these two activation steps, some uncertain metallic material was deposited on the Ag layer. With Scanning Electron Microscope (SEM) (JEOL JSM-6460 SEM, USA) and Energy Dispersive Analysis by X-Rays Spectroscopy (EDAX) (INCA Energy SEM 350, Energy Microanalysis System, England) test, this metallic material was identified as Ni. After several concentration adjustments in plating procedures, the optimal ratio for Ni electroless plating was finally obtained. The quality of the Ni layer was quite smooth and even. However, one notable thing for steel activation was that after half an hour bathing, when the Ag layer was covered by a thin layer of Ni, the steel was not necessary any more. The fiber should be removed to a piece of glass from the piece of steel in order to prevent fiber sensor from being stuck on it. Figure 4-5 shows the activation materials utilized in the Ni electroless plating process.

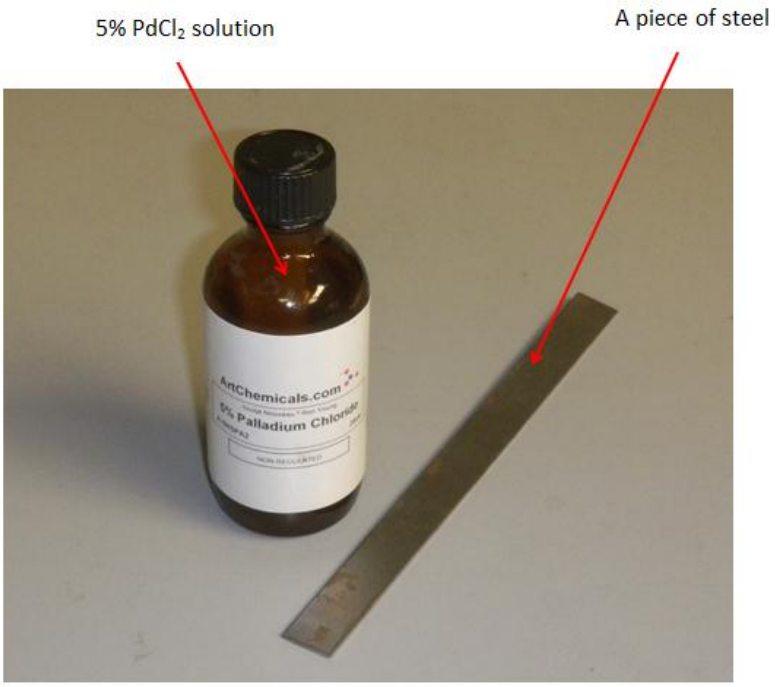

Figure 4-5 5% PdCl2 solution (ArtChemicals) and steel for activated reaction

Figure 4-6 and Figure 4-7 respectively show the Ni electroless plating solutions and when these solutions were mixed in the special ratio. The ratio for Ni electroless plating had to be experimented several times as mentioned above. We adjusted the solution at different ratios, and finally figured out the optimum ratio for Ni electroless plating on micro-scale fiber sensor. The quality of Ni that was deposited on Ag was smooth. The percentage content of Ni was almost 90%, which has been tested with SEM and EDAX process. The result was quite acceptable and satisfactory.

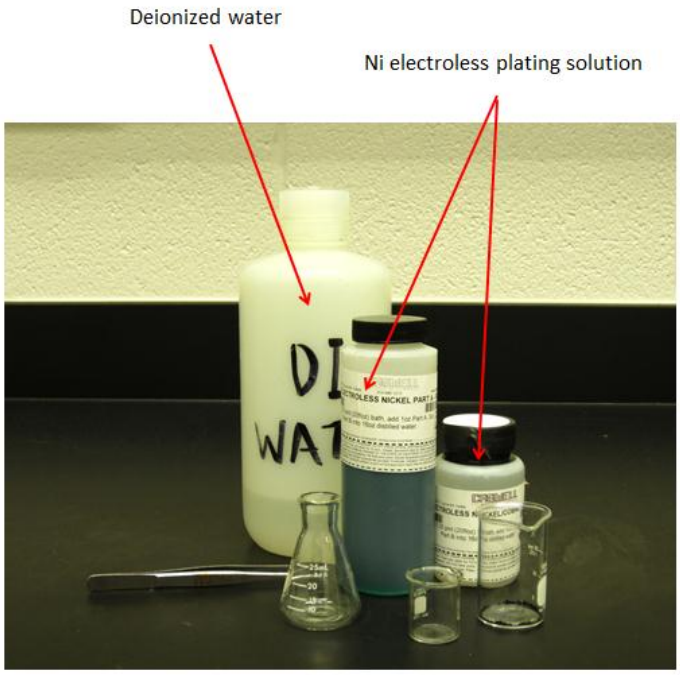

Figure 4-6 Ni electroless plating solution (Caswell, USA)

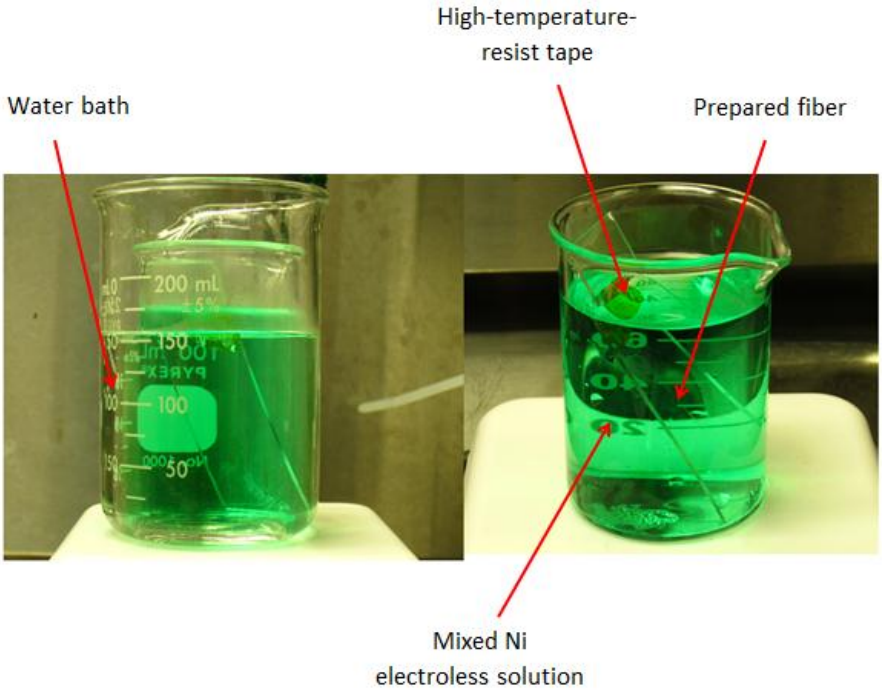

Figure 4-7 Ni electroless plating mixed solution with special ratio and heating with water bath

4.2 Fabrication methods

The methods reported in the literature for metal coating of FBGs such as magnetron sputtering, electro-winning and evaporation process are not flexible for patterning the fibers [9,33,34]. Additionally, most of them require pressure and temperature controlled chambers. In this thesis, a new method LAMM has been proposed. LAMM is classified under "Direct – Write Technologies". The Direct-Write Technology is one of the layered fabrication technologies, which means that the thin-film material would be deposited on the substrate layer by layer. In this thesis, LAMM process was used to deposit silver nano-particles layer-by-layer on the fiber surface. The Ag layer was approximately 1 μm. Then it was combined with the electroless-plating process to deposit both Ag and Ni layers on the FBGs. The details of optimum process parameters will be discussed in the following sections.

4.2.1 Laser-assisted maskless microfabrication (LAMM)

As discussed above, LAMM is a Direct – Write Technology. Compared with other methods, LAMM has a significant advantage that the deposition substrate can be either planar or irregular (cylindrical shape for instance).

4.2.1.1 LAMM process

For this study, we have developed a synchronized rotational stage for LAMM workstation to hold the fiber and spin it at controlled angular velocities. This setup enhanced the manufacturability of the Ag coating, promoting repeatability and reliability of the sensors while being used under different forces/temperatures.

The LAMM process in this thesis was used for silver thin-film fabrication. This was done in two steps; the first was the silver nano-particles deposition, and the second step was the laser-

assisted process in which adjusted laser beam was applied for heating and sintering the prior-deposited silver. We characterized the LAMM process to deposit and cure Ag nano-particles and create thicknesses in the range of 500 nm to tens of micro-meters using the layer-by-layer deposition method. The process can be performed at atmospheric pressure and does not need clean room facilities. Figure 4-8 shows LAMM workstation.

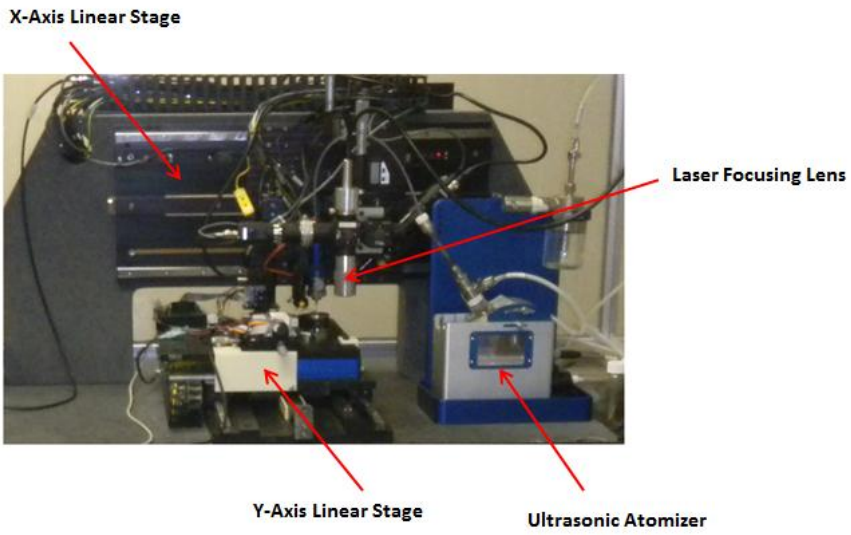

Figure 4-8 View of LAMM workstation with rotational stage for grabbing and turning the FBG

The first step has used silver nano-particles (CSD-32, Cabot Corp, Boston, MA, USA) suspended in ethylene glycol ($C_2H_4(OH)_2$) with a weight percentage of 45-55 %, called nano silver ink, to deposit the Ag thin-film. The particle size is less than 60 nm, with average of around 50nm. The silver ink was connected with atomizer system. The ink went to the deposition head as aerosol. Figure 4-9 shows the deposition head (Optomec Inc.). At the deposition head, aerosol would mix with nitrogen – sheath gas flow. This sheath gas flow rate was one of the important parameters in the LAMM process. It would help aerosol stream pass the deposition tip with stream diameter of 150 μm, which was 10% of the size of the deposition tip.

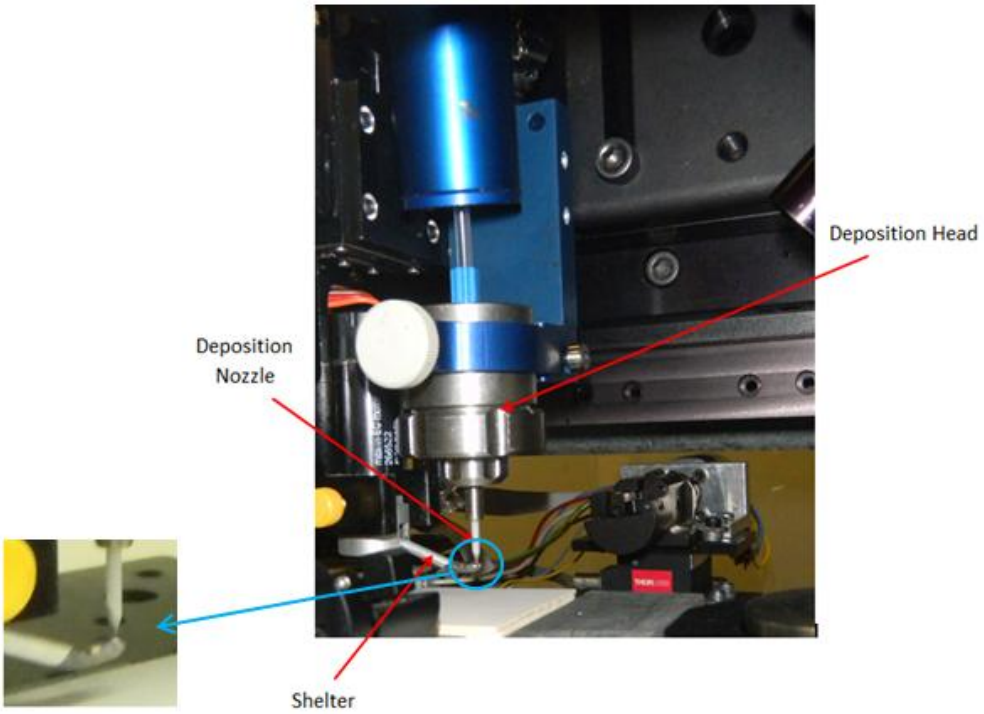

Figure 4-9 The deposition head of LAMM workstation

There is a CNC table and a thermoelectric heater below the fiber. The CNC table can be moved in any direction relative to the deposition head. The thermoelectric heater can provide a proper temperature for this layer-by-layer fabrication process.

During the Ag deposition process, as the shape of the fiber is cylindrical, a rotational stage is needed for getting an even surface. A rotator system has been developed in our lab. Figure 4-10 shows the view of the rotational stage of LAMM workstation. The fiber would be kept straight on the stage when both of its ends are mounted on the rotational stage and strained with the holders.

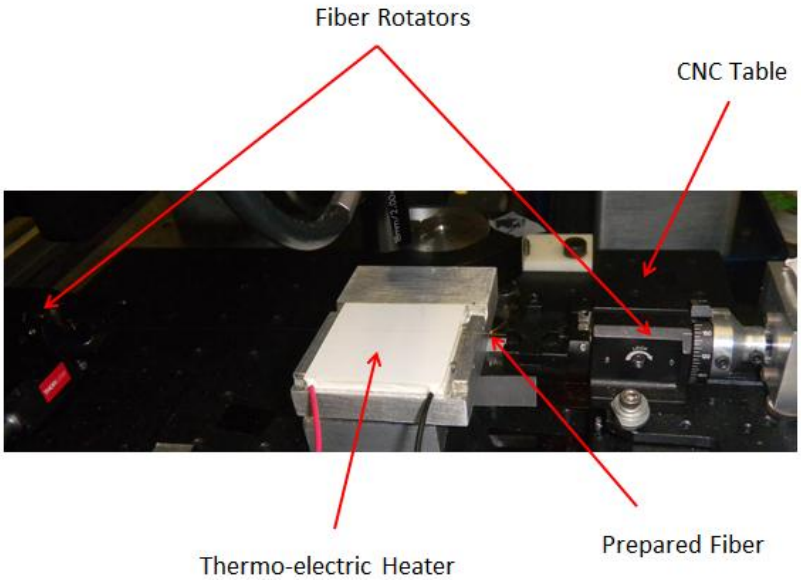

Figure 4-10 The CNC table, thermoelectric heater and rotational stage of LAMM workstation

The second step was the laser-assisted process. We used adjusted laser beam to heat and sinter the prior-deposited silver layer. An Erbium continuous beam fiber laser was used to sinter Ag nano-particles. The size of laser spot at the core of the optical fiber was 200 μm. Laser beam would scan the optical fiber at a constant speed. The laser power at the process zone is another important parameter in the LAMM process. In order to find the optimal one, we have tried three different laser powers: low-2.5W, medium-3.5W and high-4.5W in this study. The laser sintering step was followed by hot plate sintering, for half an hour at 230 ℃, to enhance agglomeration of nanoparticles.

4.2.1.2 LAMM process parameters

Parameters of LAMM process should be adjusted to obtain better surface quality. Atomizer flow rate, sheath gas flow rate, deposition velocity and rotational velocity are

parameters during the deposition process and the laser power at process zone, laser scanning speed and laser spot size are parameters for laser-assisted sintering process.

Depending on the geometrical parameters and the thickness of the deposited layer, the optimum process parameters can be determined.

Table 4-1 LAMM process parameters

Parameter	**Value**
Atomizer flow rate (cm^3/min)	10.5
Sheath gas flow rate (cm^3/min)	52
Deposition velocity (mm/s)	3
Rotational velocity for deposition (rpm)	153
Laser power at the process zone (W)	2.5, 3.5, 4.5
Laser scanning speed (mm/s)	0.25
Laser spot size at the core of the optical fiber (μm)	200
Er fiber laser wavelength (nm)	1550

After designing the geometrical parameters and mechanical properties of the deposited layer, the process parameters can be determined. In LAMM process, the main characteristics that would affect the process parameters are the geometrical features and the thickness of the deposited layer. In this research, we need to deposit a thin silver layer around cylindrical fiber. Since the processing parameters were first investigated for planar substrates, parameters for this cylindrical fiber substrate needed to be transferred from planar processing parameters. The optimum parameters of LAMM for deposition of thin Ag films on fiber and laser sintering are listed in Table 4-1 [56]. Different laser powers have been experimented to figure out the proper laser power for sintering process with optimum quality.

4.2.1.3 LAMM experimental procedures

The first step of LAMM was placing the prepared fiber on fiber rotators and fixing both ends to keep the prepared fiber straight. The second step was checking the deposition quality over the thermoelectric heater. After this, the deposition process could be started on the fiber at a high rotation speed.

The fiber is cylindrical; if it were not rotating, the silver ink could not deposit on the fiber evenly. The thin silver layer was deposited on rotating fiber by moving the deposition head in a programmed path.

Since the fiber surface is not planar, only the side exposed under the deposition head would be deposited with silver nanoparticles. In order to keep the deposition surface uniform, the optical fiber was rotating at a high rotational velocity. Based on the CNC table's moving speed, the whole process of depositing one layer of silver took approximately 30 minutes. Two times deposition were generally required. The thickness of the silver layer was 1 μm.

4.2.1.4 Sintering process of silver nanoparticles

Because the silver on the surface of optical fiber hasn't been sintered yet, the silver couldn't adhere to fiber surface tightly. If the surface is scratched, the silver might be removed and cause non-uniformity in the silver surface layer. Laser assisted sintering process was required here.

Laser assisted process is the second step in LAMM process. Erbium beam fiber laser was utilized for heating and sintering the silver layer deposition. The laser spot size at the core of fiber was adjusted to 200 μm and the scanning velocity was 0.25 mm/s constantly. In order to find the most proper laser power for sintering process, three different laser powers were applied:

2.5W, 3.5W and 4.5W, defined as low power, medium power and high power respectively. After the silver layer has been sintered by laser, the optical fiber was removed from the rotators carefully. This laser sintering step was followed by another half an hour hot plate sintering at 230 ℃. This following sintering step was aimed at increasing the agglomeration of nanoparticles.

There are two mechanisms of sintering process. The difference between these two mechanisms is the strength of the particles' bonds. With stronger bond, the coalescence mechanism will work. The particles will be fused and produced through "neck-shape" structures to a single new big particle whose surface area has been changed. However, if the bonds between particles are weaker, particles will be compacted and rearranged [62, 63]. The sintering process in this study performed as the first main sintering mechanism. Figure 4-11 shows the main sintering mechanism of this research [62, 63].

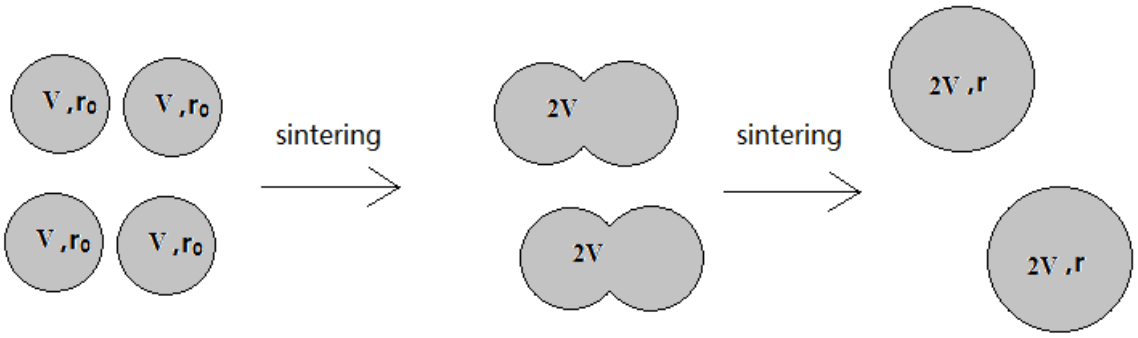

Figure 4-11 The mechanism of sintering process [59, 60]

4.2.2 Electroless plating for thin metallic film deposition

After depositing the conductive Ag layer, the thicker Ni layer could be coated. There are several ways to coat Ni layer on the conductive layer. The most common way is electroplating. Instead of vacuum techniques and high temperature requiring methods, Sandlin et al. [18]

applied electroplating process to deposit Ni layer on the thin conductive layer. In their electroplating process, a PE-plastic holder was required for holding the pre-coated fiber, and current feed cable was also needed to be in contact with the conductive layer. The disadvantage of this method was that the contact between fiber's conductive layer and the cable had to be very accurate. If there was not a tight electrical contact, the conductive layer might be removed from fiber during the electroplating process. Li et al. [33] reported magnetron sputtering to coat FBG with a thin Ti-Ni film, and then applied electroplating to deposit another 0.5-1 mm Ni layer on the pre-coated FBG. Finally, the FBG was embedded into the metallic structure. The thicker Ni layer could both protect FBG sensor from high temperature embedding process (laser fusion and casting process for instance), and enhance FBG's thermal sensitivity. However, the only disadvantage of this method was the inaccurate strain sensitivity caused by residual stress.

Feng et al. [34, 37] utilized electroless plating to deposit a Cu layer on FBG as the conductive layer and then applied electroplating to deposit Ni layer on it. With the protection by Ni layer, the pre-coated FBG could be embedded within steel structure by high temperature process. And the developed FBG sensor showed higher temperature repeatability and higher thermal sensitivity.

Nowadays, the most common method to deposit Ni on the conductive layer is electroplating. However, current, cable and solutions are required in this method, and the accurate contact between cable and conductive layer is so important that it affects the quality of Ni coating. If the contact is not close enough, even the conductive layer may be removed from the optical fiber during the Ni^{2+} bathing process. Therefore, in this thesis, we applied Ni electroless plating process for Ni layer deposition. During electroless plating process, neither cable nor current is required; only Ni^{2+} solution and activation materials are needed. With respect

to electroplating, this method is simple, cheap and easily controlled. However, the solution properties belong to CASWELL Inc. USA, and we just know that Ni^{2+} has been included in the solution, other chemicals, their concentration and ratio are unknown.

4.2.2.1 The optimal ratio for electroless plating solution

The solution and materials for electroless plating were provided by CASWELL Inc. USA. The ratio of Ni bathing mentioned in their introduction book was not concentrated enough. That ratio is applicable on large structures. However, the optical fiber is a micro-scale structure, therefore, the dilute solution could not deposit Ni particles on the conductive layer. We adjusted the ratio several times and finally figured out the most effective and proper concentration for Ni electroless plating, which is water: Part B: Part A=8:3:1. The property of the solution belongs to the CASWELL Inc. USA. The quality of the results will be addressed in the following chapter.

4.2.2.2 Preparation and activation procedures

In order to obtain high quality of Ni plating, the preparation steps and the activation procedures are important.

Even after adjusting the solution ratio, Ni did not deposit on the FBG in the beginning. After literature review, it was figured out that some activation procedures should be carried out before Ni electroless plating. Based on many experiments, a two-step activation method was developed for high quality Ni deposition.

The activation method is: before Ni plating process, the fiber coated with Ag was immersed in a solution of 10% H_2SO_4 at 65℃ for 5 minutes for acid cleaning. This step would clean the dust and the oxide on the optical fiber's surface. Then, the fiber was immersed in deionized water for rinsing the acid. Prior to the Ni plating, to decrease the potential barrier for

Ni deposition, one additional step was required. To do that, the FBG sensor was immersed in 5% $PdCl_2$ solution for 5 minutes at 50 ℃ and a thin Pd activation layer was deposited on the Ag surface [60, 61]. After 5 minutes, the fiber was again needed to be rinsed in deionized water.

One more activation step was using steel to activate the Ni electroless plating. The optical fiber was placed on a piece of steel and in contact with it as tight as possible. However, in order to keep the thickness of Ni uniform, optical fiber could not stay on the steel during the whole Ni bath. After a thin Ni layer was deposited on the fiber's surface, the steel could be replaced by a piece of glass.

4.2.2.3 Electroless plating procedures

Ni electroless plating does not require anodes, electrical current and power supply. This process just needs mixing solutions together and heating them up to the exact temperature (90.56 ℃), and then plating the part by immersing it in the mixed solutions [64].

The reactions of Ni electroless plating have been introduced in [65],

$$H_2PO_2^- + H_2O \rightarrow H_2PO_3^- + H_2$$

$$Ni^{2+} + H_2PO_2 + H_2O \rightarrow Ni + H_2PO_3^- + 2H^+$$

$$H_2PO_2^- + H^+ \rightarrow P + OH^- + H_2O$$

During the plating, the fiber was first placed on a piece of steel and taped by high-temperature-resistant tape at both ends to ensure that the contact points were established. The steel was used as a material to activate the electroless plating process. The plating solution was heated to 90 ℃ with a water bath and the steel with mounted fiber was immersed in the bath for half an hour. In this half an hour, Ni was deposited as a thin layer all over the fiber. After 30

minutes, the steel was taken out of the Ni bath. In order to make the deposition with a better quality and uniform thickness, the FBG sensor was moved to a piece of glass for an extra one and a half hour Ni plating. Figure 4-12 shows all the procedural steps of the Ni electroless plating process. The first five are activation methods, the rest of them are Ni electroless plating process.

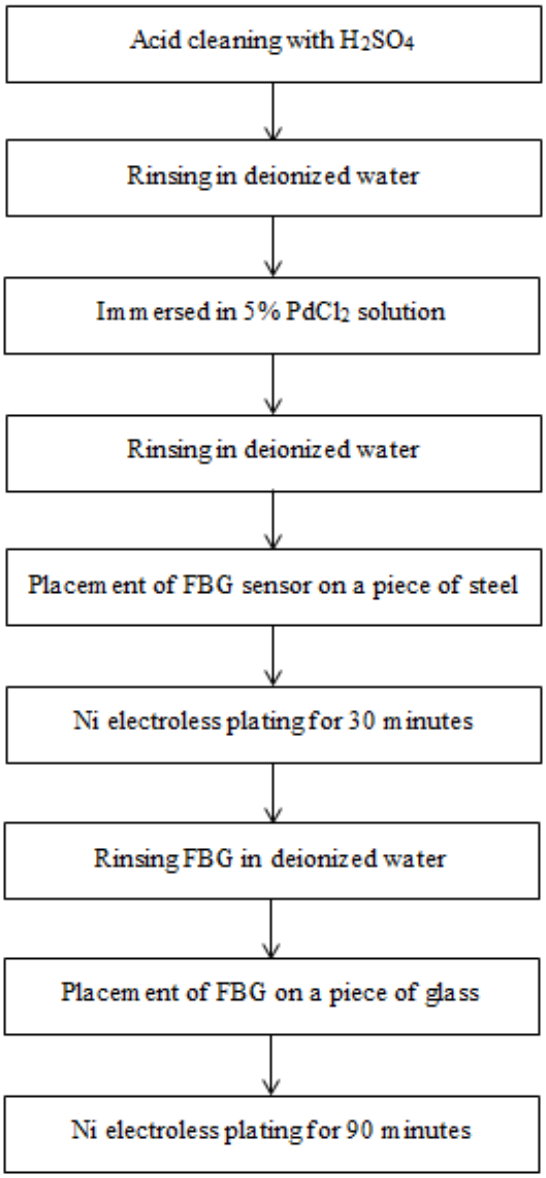

Figure 4-12 Procedures of Ni electroless plating on FBG sensor

4.3 Characterization methods

Characterizations of the Ni and Ag layers were performed by the Scanning Electron Microscope (SEM) (JEOL JSM-6460 SEM, USA) and Energy Dispersive Analysis by X-Rays Spectroscopy (EDAX) (INCA Energy SEM 350, Energy Microanalysis System, England). The SEM and EDAX results will be shown in the following chapter.

4.4 Sensor calibration and packaging

A calibration setup has been developed by our research group to achieve the characteristic curves of the sensors [59, 66]. In the calibration procedure, axial force is applied on the optical fiber by a linear micro-stage with a positional resolution of 0.005μm and a minimum incremental motion of 0.1μm in a temperature controlled chamber, and the load/displacement sensor records the axial force with a resolution of 0.03N [66]. To calibrate the sensor without damaging it, FBG is placed on a special package, which consists of two parts made of Invar-36 (FeNi36), because of Invar-36's low thermal expansion coefficient [66].

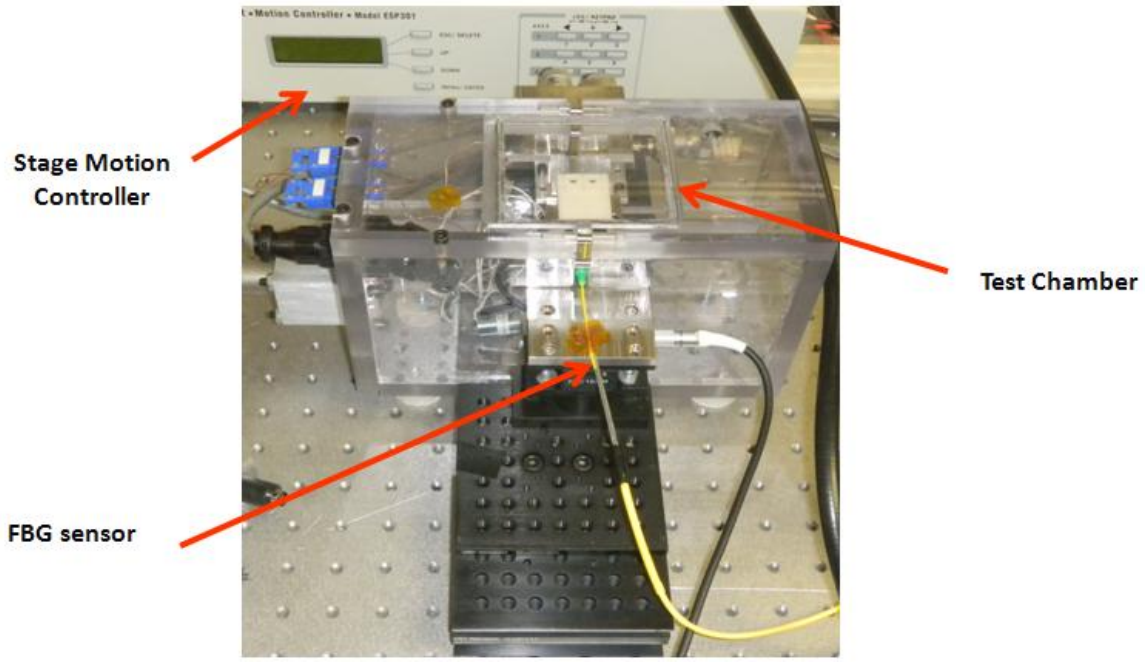

Figure 4-13 Calibration setup and package for FBG

A virtual control panel designed in LabVIEW controls the calibration setup as shown in Figure 4-14 [66]. When the packaging FBG sensor is connected to the interrogator, the signal and wavelength of sensor is shown. The three parallel windows show inlet, sensor and free thermocouple temperature respectively. This program was developed by our research group.

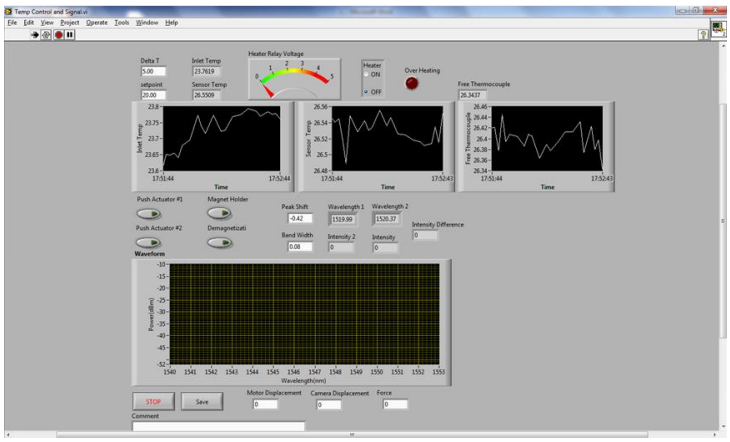

Figure 4-14 LabVIEW control window

4.5 Summary

This chapter has discussed the LAMM process and Ni electroless plating process. Characterized parameters of LAMM for thin metallic film deposition on FBG sensor and coated FBG with Ag-Ni coating layer by LAMM and nickel electroless plating process. The experiment target is using Ag-Ni thin-film layer on FBG for both protection and sensitivity increasing.

Chapter 5

Experimental results

In this chapter, the experimental results are presented. As described before, the LAMM was used to deposit the conductive Ag layer followed by Ni electroless plating to deposit a 33μm Ni layer on the thin Ag film. The process can be separated into the LAMM process and Electro-less plating process. This chapter discusses the effect of laser powers on the Ag layer and also discloses the performance of the coated FBG sensor under thermal and loading strains.

5.1 LAMM process results

As discussed above, LAMM is a Direct–Write Technologies. LAMM process was used in this thesis for silver thin-film fabrication. First, the silver nano-particles were deposited on the optical fiber, then laser-assisted process was used in which the adjustment laser beam was applied for heating and sintering the prior-deposited silver deposition. We characterized the LAMM process to deposit and cure Ag nano-particles and create thicknesses in the range of 500 nm to tens of micro-meters using the layer-by-layer deposition method. The process can be performed at atmospheric pressure and does not need clean room facilities.

However, in order to obtain the optimum quality of metallic surfaces, different laser powers have been tested during the sintering process. Low, medium and high laser power referring to 2.5W, 3.5W and 4.5W respectively has been applied for the same thickness Ag layer sintering. After the analysis of the microstructure, the optimum laser power was obtained. Also, the effect of the hot plate sintering was considered.

The LAMM process results are the characterizations of the Ag layers which were performed by Scanning Electron Microscope (SEM) (JEOL JSM-6460 SEM, USA) and Energy Dispersive Analysis by X-Rays Spectroscopy (EDAX) (INCA Energy SEM 350, Energy Microanalysis System, England).

5.1.1 Microstructure tests and analysis

The LAMM process, one of the Direct-Write Technologies, has a significant advantage that the deposition substrate can be either planar or irregular (cylinder for instance). After depositing a thin layer of Ag, the sintering process by laser was followed. In this thesis, three samples have been made. Each optical fiber has been prepared by the same procedure and an Ag layer with the same thickness has been deposited on all of them.

Then, samples have been sintered with different laser powers of 2.5W, 3.5W and 4.5W, referred to as low, medium and high laser power. With the same laser scanning speed and the same beam spot size, different sintering quality could be observed. The laser power is laser power at the process zone. However, the medium laser sintering process (3.5W) followed extra 30 minutes physical hot plate sintering at 230℃, in order to test the effect of the physical high temperature sintering.

By the mechanism of laser sintering, the nanoparticles will be lightly sintered at low laser power and over-sintered at high laser power. In order to figure out the proper laser power, different laser powers' microstructure figures were obtained for observation.

5.1.2 Results

The LAMM process results were analysed by the optical microscope, SEM and EDAX as follows. Figure 5-1 shows the characterizations of the Ag layers on FBG sensor from optical microscope. The darker layer was the Ag layer coated on the optical fiber. And at the left hand side, it is the fiber's polymer cladding.

Ag conductive layer should be deposited on the FBG's Bragg gratings directly. During the preparation process, part of polymer coating was removed from fiber for future Ag layer deposition. Ag has been deposited by M^3D machine, in order to keep the quality of Ag layer smooth and uniform. This deposition process has been processed twice. The thickness of the Ag conductive layer is 1 μm approximately, adhered tightly to the fiber, whose diameter is 125 μm.

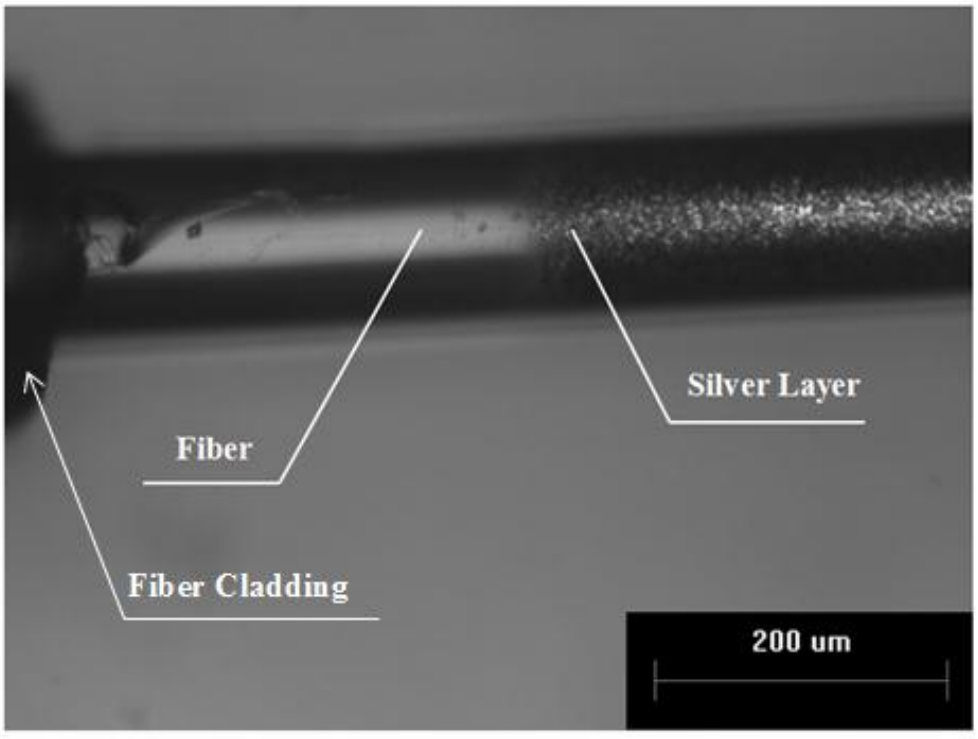

Figure 5-1 Optical microscope image of optical fiber sensors with Ag coating

After laser sintering process, the image of the optical fiber and its Ag coating has been captured by the SEM.

Figure 5-2 shows the fiber coated with silver before electroless plating with high power (4.5W) sintering. Figure 5-3 shows the low power (2.5W) sintering of the fiber with silver coating. Figure 5-4 shows the fiber coated with silver with medium laser power (3.5W) sintering and followed by half an hour hot plate sintering at 230 ℃.

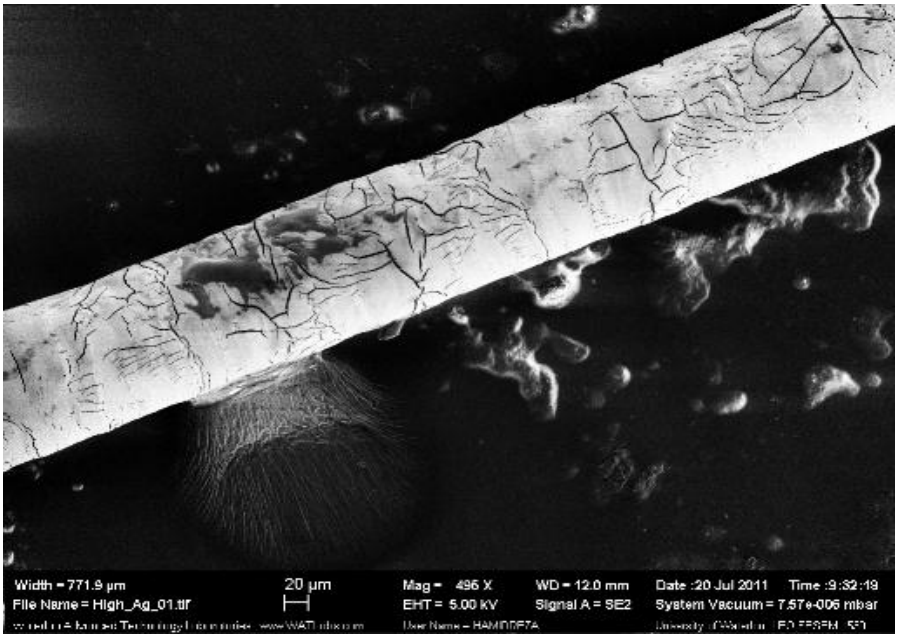

Figure 5-2 SEM electron image of optical fiber coated with thin silver sintered by high laser power (4.5W)

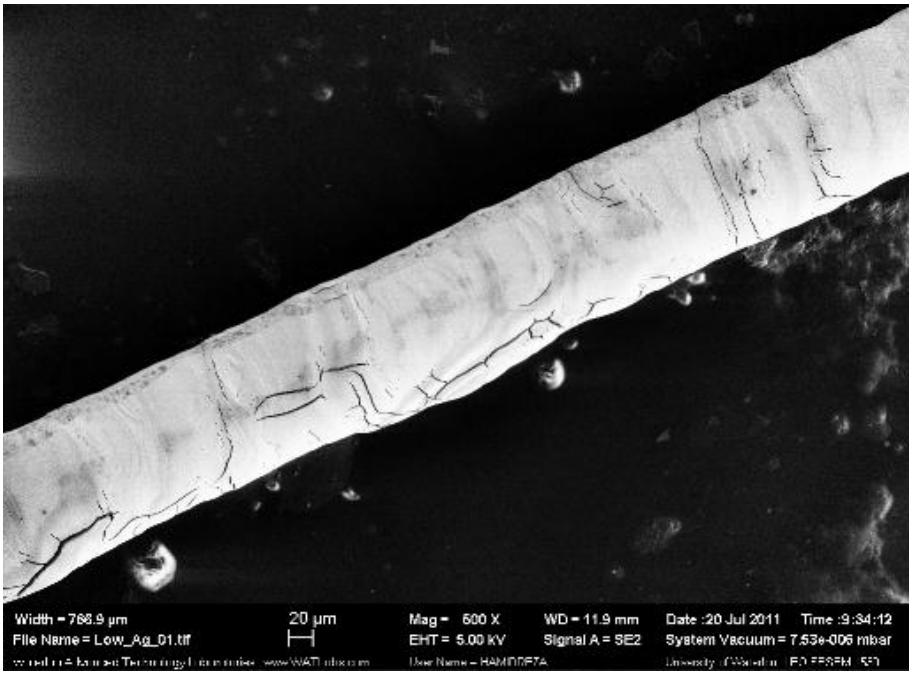

Figure 5-3 SEM electron image of optical fiber coated with thin silver sintered by low laser power (2.5W)

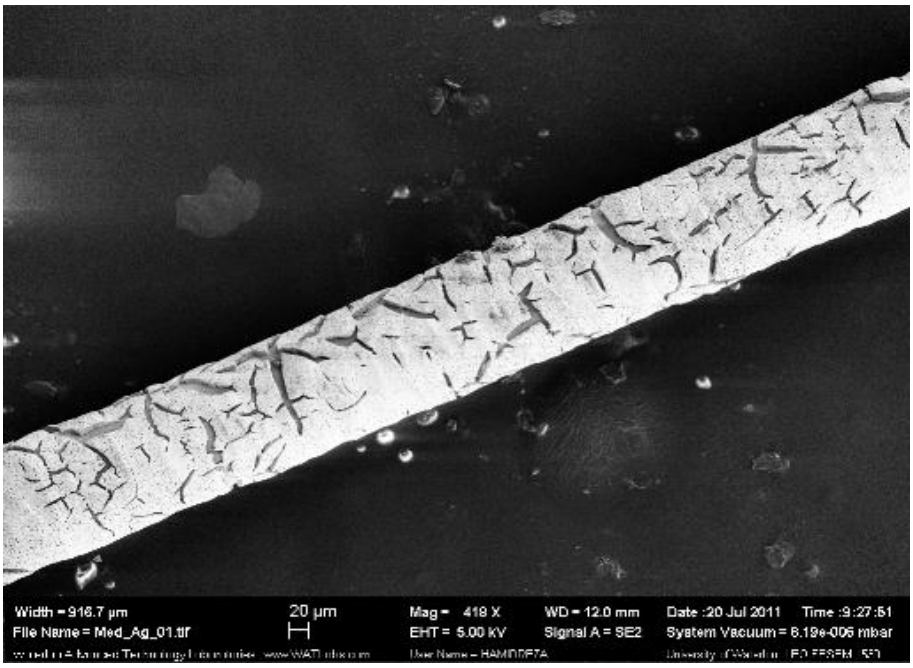

Figure 5-4 SEM electron image of optical fiber coated with thin silver sintered by medium laser power (3.5W) and followed with hot plate sintering at 230 ℃

As seen from the figures above, the high power (4.5W) sintering has created more cracks on the silver surface compared to the low power (2.5W). The medium power (3.5W) sintered sample which was also sintered by a hot plate at 230℃ for 30 minutes showed over-sintering on the Ag surface. The crack formation may be a result of over-sintering and possible shrinkage in the agglomerated Ag.

The cracks of medium power sintering were less than the high power (4.5W) sintering, however, the size of those cracks were much bigger than the high power (4.5W) sintering. The high power created narrow cracks. While the medium power sintering did not create cracks as much as high power one, the 30 minutes hot plate sintering broadened those cracks. The laser sintering added with hot plate high temperature sintering resulted in over-sintered Ag surface.

Figure 5-5 shows highly magnified SEM images of the Ag surface. According to this figure, the silver film has cracks and holes showing that it has been over-sintered.

According to the figures, the medium laser power (3.5W) sintered fiber which was also sintered by a hot plate at 230℃ for 30 minutes exhibits significant cracks. However, the figure shows that the Ag surface has been sintered completely. The crack formation may be a result of over-sintering and possible shrinkage and residual stress in the agglomerated Ag. It can be controlled by adjusting the sintering temperature and the thickness of the Ag coating. Although some cracks are distinguishable, from the results and figures obtained later, the cracks did not exhibit any counter productivity during Ni plating. What's more, the results of the EDAX process after Ni electroless plating process, the medium laser power sintering process followed with 30 minutes hot plate sintering at 230℃, showed the highest contents of Ni elements. This

phenomenon showed that if the high temperature hot plate sintering process could be controlled properly, it might help the Ni surface plate on the conductive layer more effectively.

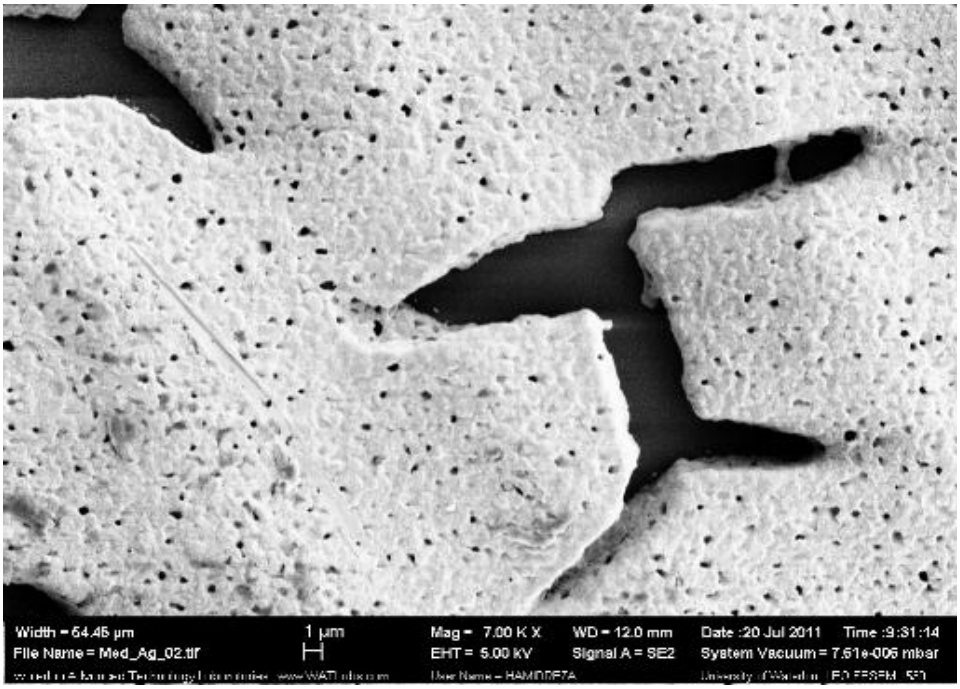

Figure 5-5 SEM electron image of cracks on over-sintered silver surface

5.2 Electroless plating process results

After optical fiber has been deposited with Ag conductive layer and sintering is complete, the Ni electroless plating was applied for both protection and thermal sensitivity enhancement.

As Chapter 4 discussed, before the electroless plating, the procedures of acid cleaning and activation process have been applied on the Ag coated optical fiber. Acid cleaning was used for cleaning the Ag surface which might produce slight oxide. Activation step was applied to decrease the potential barrier for Ni deposition. The optical fiber was immersed in 5% $PdCl_2$ solution for 5 minutes at 50 ℃ so that Pd^{2+} particles would adhere on the Ag surface and form a thin activation Pd^{2+} layer, in order to reduce the potential barrier for Ni plating.

During the plating process, the fiber was placed on a piece of steel and taped with high-temperature-resistant tape at both ends to ensure that the contact areas are established. This was another activation step to promote easy Ni electroless plating.

The whole electroless plating was heated by water bath, and the temperature of the plating solution was kept at 90 ℃. The steel activated the fiber in the bath at the first half an hour. Because Ni electroless plating worked both on Ag surface and steel surface, in order to keep the Ni coating uniform and smooth, the steel was removed after a thin Ni layer was deposited on Ag. Then, the FBG sensor was mounted on a piece of glass for another extra 90 minutes Ni plating to get thicker. Had FBG sensor been kept on the steel for the whole two hours, the part of the sensor in contact with steel might not have been plated. Figure 5-6 shows the cross-sections of the sensor when kept on and removed from the steel.

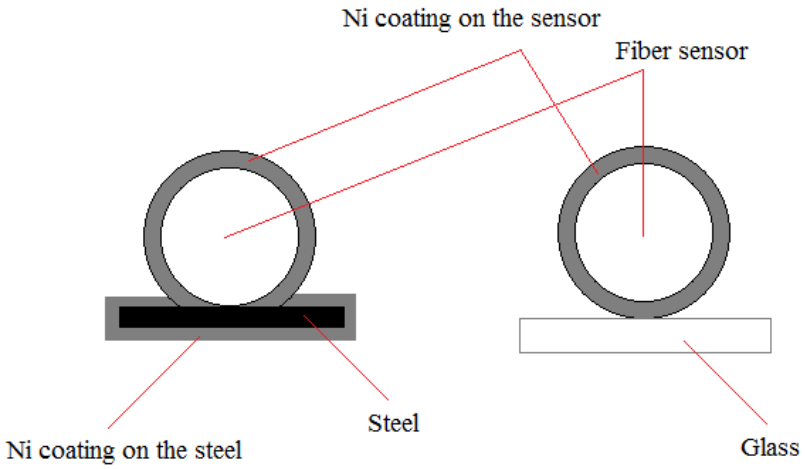

(a) (b)

Figure 5-6 (a) Cross-section of the sensor is electroless plated on the steel (b) Cross-section of the sensor is electroless plated on the glass

5.2.2 Microstructure tests and analysis

The thickness of Ni plating is dependent on the time of Ni bathing. To define the accurate rate between the enhancement of Ni thickness and the Ni bathing time, several experiments were done to test the thickness of Ni which is affected by the duration of electroless plating. Figure 5-7 shows the relation between Ni bathing time and the Ni layer thickness. As time increased, the thickness of Ni grew. The rate of Ni thickness enhancement is 18 μm/hour approximately. Depending on this rate, the thickness of Ni could be controlled. As the theoretical result discussed in Chapter 4, the optimum thickness of Ni coating is in the range of 30 to 40 μm.

According to the range, the Ni bathing time should be 2 hours approximately.

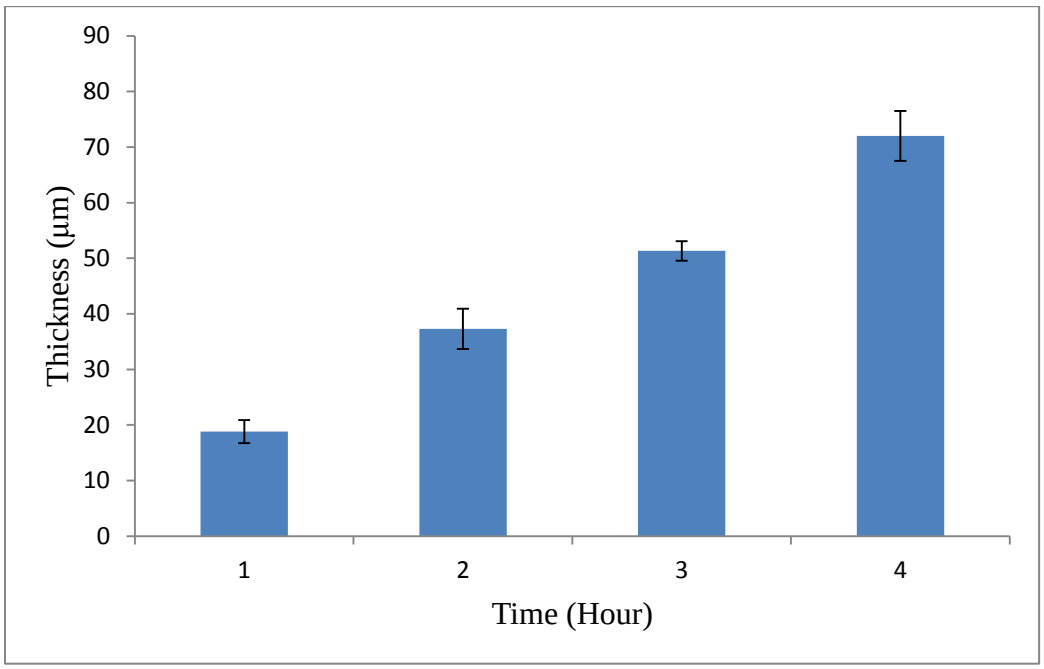

Figure 5-7 Ni layer thickness as a function of the Ni electroless plating time

5.2.2 Results

After the conductive Ag layer has been deposited and sintered on the optical fiber, Ni electroless plating was applied on the Ag layer. This process could provide both protection and temperature sensitivity enhancement. After the cleaning and activation steps, the fiber was mounted on a piece of regular steel and taped by high-temperature-resistant tape at both ends in the Ni bath (90℃) for activation purpose. 30 minutes later, the optical fiber was removed from the steel and mounted on a piece of clean glass for another 90 minutes in a Ni bath (90℃) which was also heated by water bath. At last, the Ni thickness turned to be 33μm, belonging to the optimum range of 30 μm to 40 μm.

Ni electroless plating process results were also analysed by the optical microscope, SEM and EDAX. Figure 5-8 shows the characteristics of the Ni layers as seen in the optical microscope. The darker and thicker layer is the Ni layer coated on the optical fiber and the conductive Ag layer. The diameter of the fiber is 122-125 μm approximately, and the diameter of the fiber with Ni coating is 190 μm, accordingly the thickness of Ni can be calculated. Then, by several more measurements, the thickness of Ni coating was found to be 33 μm. From the figure obtained from optical microscope, the quality of Ni coating is quite smooth and uniform. However, in order to achieve more details about the surface, SEM test is required.

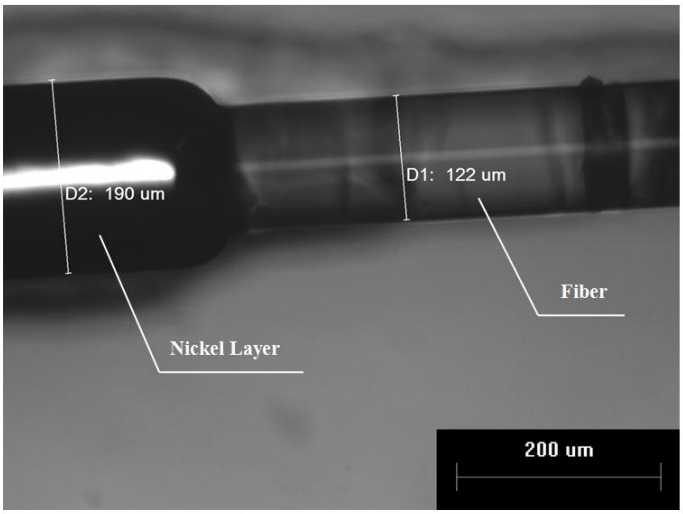

Figure 5-8 Optical microscope image of optical fiber sensor with Ni coating

The image of the optical fiber and its Ni coating has also been captured by the SEM. Figure 5-9 shows the fiber coated with Ni-Ag with high power (4.5W) sintered silver. Figure 5-10 shows the low power (2.5W) sintering result after Ni plating. Figure 5-11 shows the Ni plated fiber which was sintered by medium power (3.5W) and followed by half an hour hot plate sintering at 230 ℃.

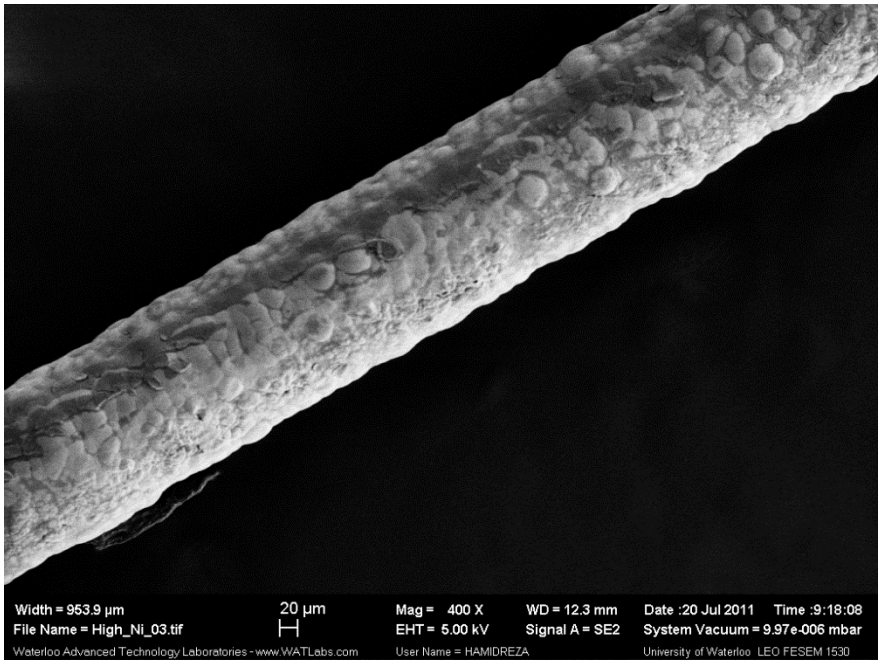

Figure 5-9 SEM electron image of optical fiber coated with 34µm nickel on high laser power (4.5W) sintered silver

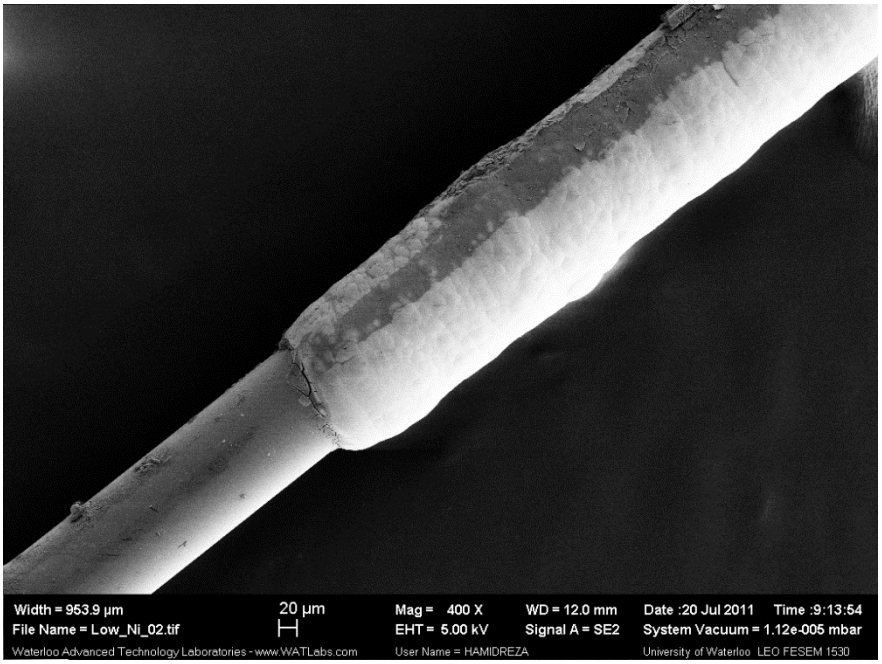

Figure 5-10 SEM electron image of optical fiber coated with 34µm nickel on low laser power (2.5W) sintered silver

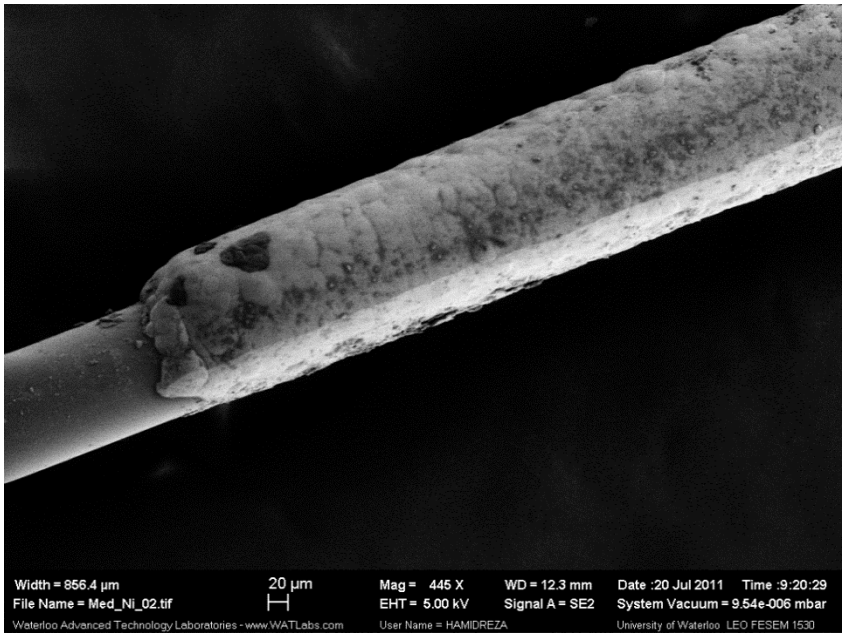

Figure 5-11 SEM electron image of optical fiber coated with 34µm nickel on medium laser power (2.5W) sintered and hot plate sintered silver

Comparing low (2.5W) and high (4.5W) power laser sintered optical fiber samples, the low laser power sintering shows better plating result, with less bumps, cracks and a smoother surface. However, the medium laser power sintered sample also shows quite good quality; the surface of the Ni is even and smooth, with less porosity and cracks. These results showed that the hot plate sintering process could also work well. However, when compared with the low laser power sintered sample, the medium laser power sintered followed with hot plate sintered sample did not seem as smooth as the low laser power sample. These results may need future tests and measurements in order to find out the optimum laser power and whether hot plate sintering process is required or not.

Therefore, the EDAX tests have been performed to detect the quality and contents of the Ni layer of each sample.

By using EDAX, the chemical composition of the deposited layers can be detected.

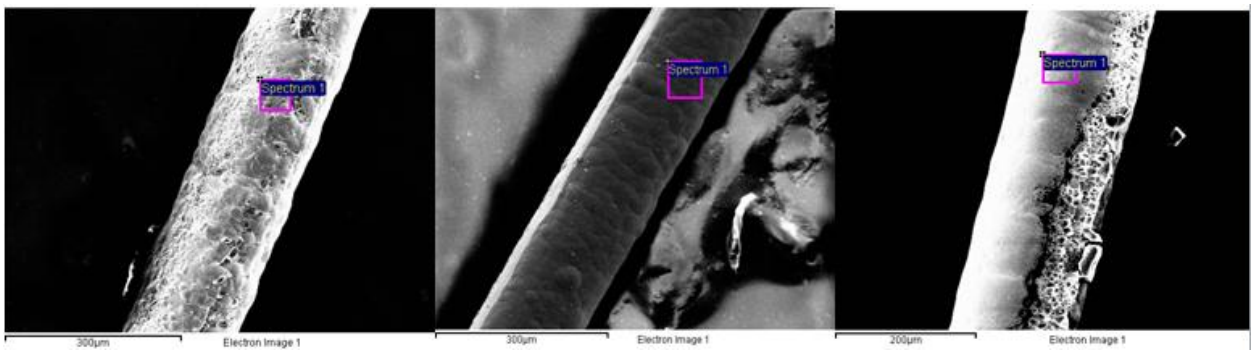

(a) (b) (c)

Figure 5-12 (a) EDAX graphs high laser sintering fiber, (b) EDAX graphs medium laser sintering fiber and (c) EDAX graphs low laser sintering fiber

Table 5-1 The contents of Ni elements at different laser power sintering from EDAX data

Laser power	Ni (wt%)
High power (4.5W)	81.09
Medium power (3.5W)	91.34
Low power (2.5W)	85.56

Figure 5-12 shows the EDAX graphs of high, medium and low laser sintering fibers, and Table 5-1 suggests that with 3.5W laser power, the Ag surface shows lower porosity and cracks and better quality of Ni-Ag layer. The Ni content is also the highest compared with samples sintered by other level laser powers.

We observed that if we have a post-annealing process for about half an hour using the hot plate sintering process after the laser sintering process, the Ni content of the sample increases to 100% within the spectrum area of 125 by 125 micron as shown in Figure 5-14 and Figure 5-15.

Figure 5-13 shows the EDAX graph of FBG sensor coated with Ni-Ag bi-material layer and sintered by both medium laser power and hot plate. We have chosen 4 spectrums. Each content is shown in Table 5-2.

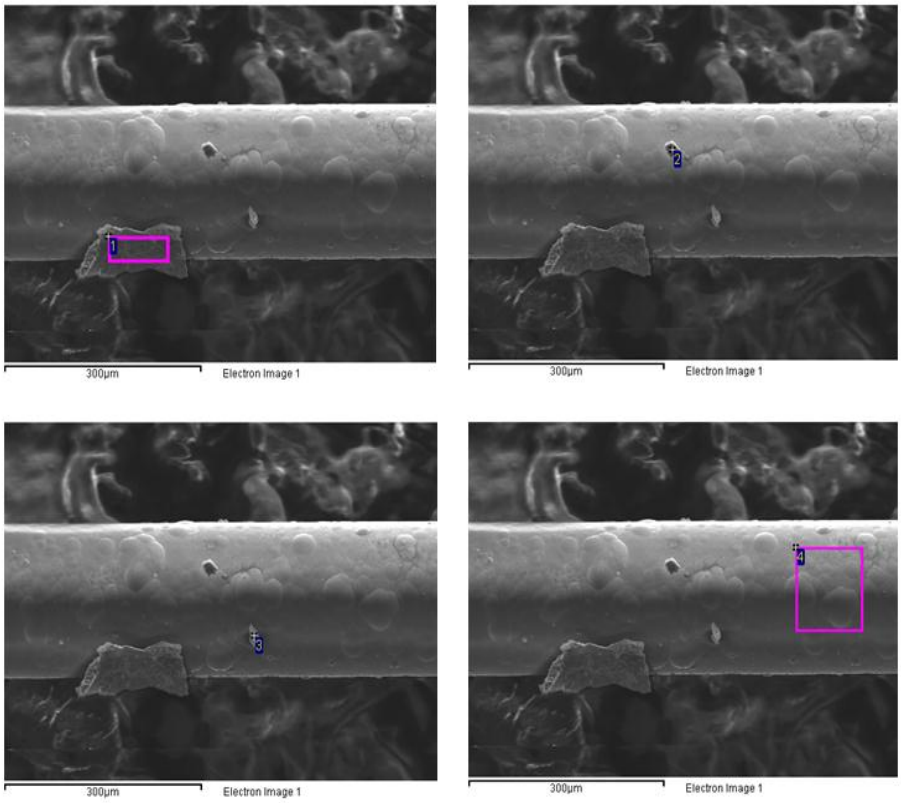

Figure 5-13 EDAX electron image of optical fiber sensor with 4 spectrums

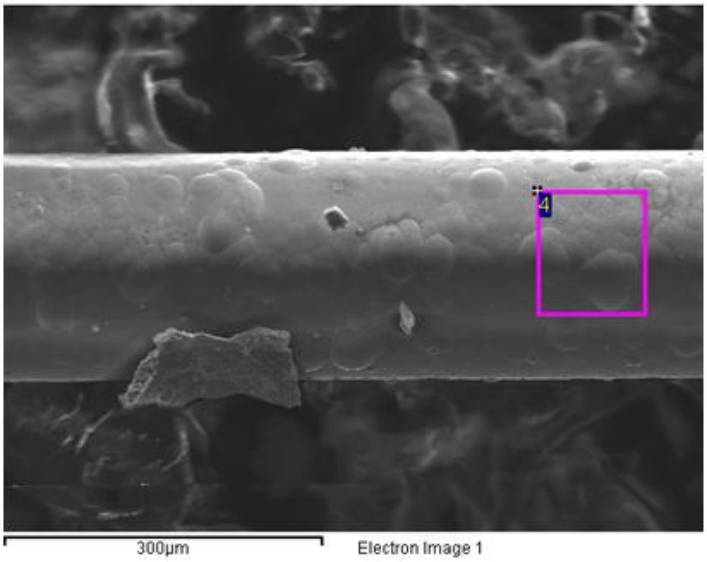

Figure 5-14 EDAX electron image of optical fiber sensor with the fourth spectrum

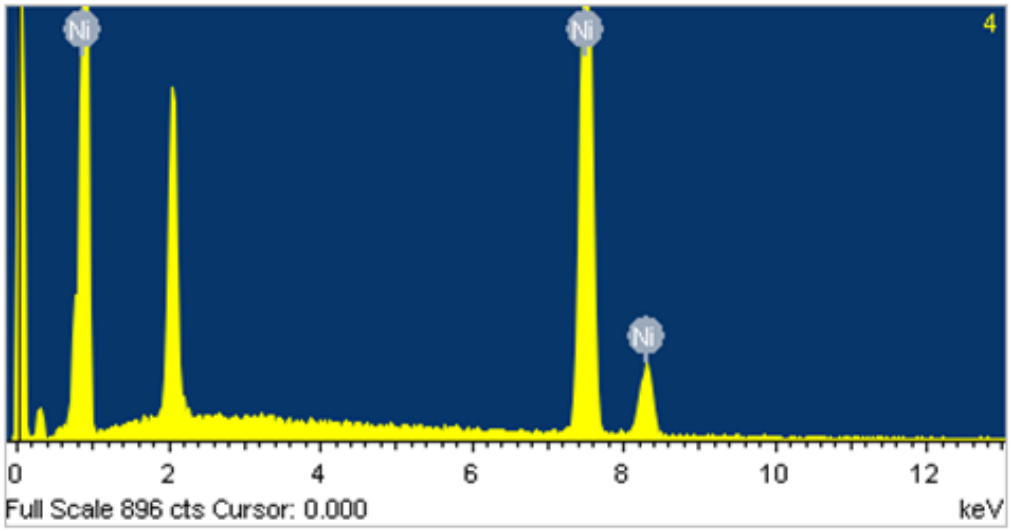

Figure 5-15 The contents of Ni for the fourth spectrum

Table 5-2 The contents of Ni elements

Spectrum	Ni (wt%)
1	3.46
2	75.94

3	90.42
4	100

Table 5-2 shows the contents of Ni elements of each spectrum form Figure 5-13. For the fourth one, the Ni content increases as high as 100% within the spectrum area of 125 by 125 microns. However, when comparing other result with spectrum 1, the Ni content is only 3.46%. We observed Figure 5-13 again and found out that the spectrum 1 has been captured on a bump adhered on the optical fiber. The content of Ni there was really low, but the content of Fe detected by EDAX was 95.28%. Based on this data, we could ensure that the bump was a piece of steel that had adhered on the Ni coating surface. The reason was that the sensor had been mounted on a piece of steel for activation step, and even though the steel had been removed, some small pieces of steel might still have been in the solution. This phenomenon showed one of the disadvantages of electroless plating.

Spectrum 2, 3 and 4 presented good quality of the Ni surface. Spectrum 2 and 3 also showed high contents of Ni elements to defend this result, but spectrum 2 and 3 were too small to define the Ni surface and only spectrum 4 was a strong definition for Ni coating. The 33 μm thickness is completely formed by nickel.

5.3 Summary

This chapter presented the experimental results. 1 μm Ag layer and 33 μm Ni layer was deposited on FBG. The effect of laser powers on Ag layer was discussed and the qualities of Ni layer on different laser power sintered Ag layer were compared.

Chapter 6

Packaging and sensing results

In this chapter, the packaging and calibration process of the bi-material coated sensor will be discussed. Some experiments have been conducted to sense the bi-material coating FBG sensor's thermal and force sensitivity. The experimental results have been compared with the theoretical results and the difference has been discussed.

6.1 Packaging and calibration the FBG sensor

6.1.1 Sensor connector preparation

Before the FBG sensor is calibrated, it needs a connector for attachment to the interrogator.

First, the FBG sensor needed to be glued inside the connector. Then, we used a connector oven as depicted in Figure 6-1, to dry the glue at 100 ℃ for 30 minutes. Next, the sensor with the connector was polished on four different kinds of polishing paper (5 μm grit, 3 μm grit, 2 μm grit and 0.3 μm grit polishing paper), as shown in Figure 6-2. Last, we inserted the sensor into 900 μm furcation tubing, and then covered it with 3mm furcation tubing [59].

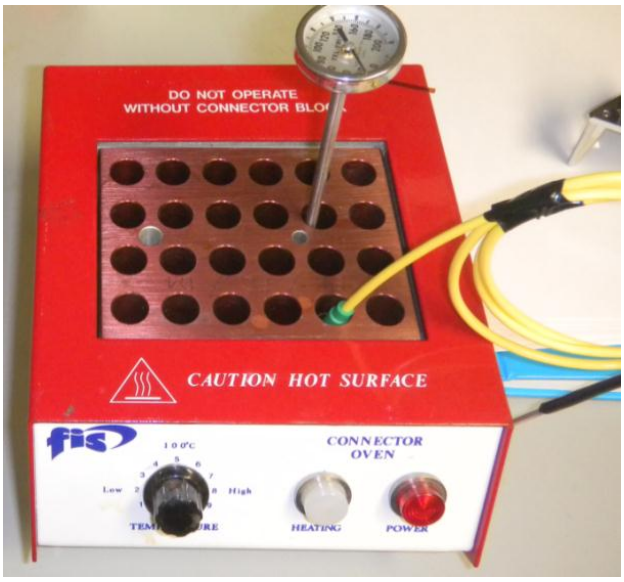

Figure 6-1 Connector oven

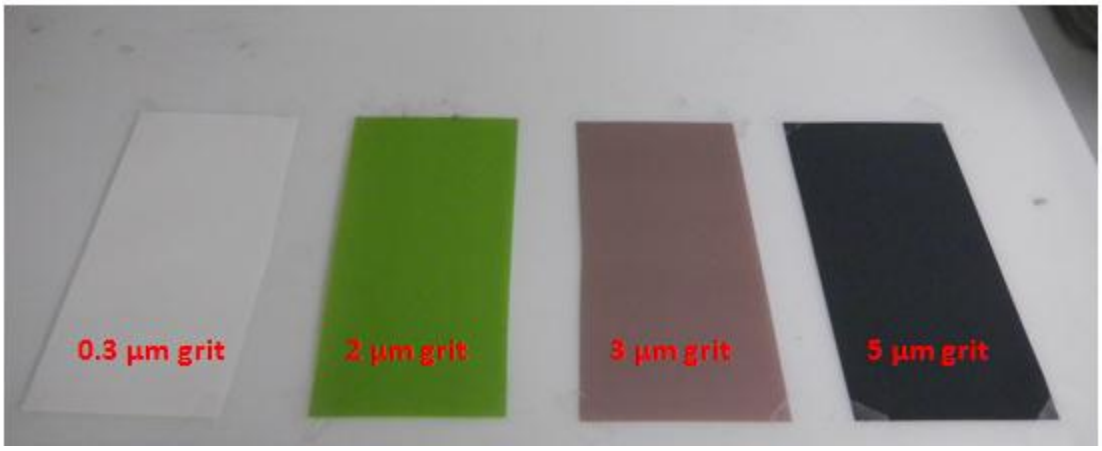

Figure 6-2 Polishing papers for connector polish

6.1.2 Packaging procedure

During the packaging procedure, the sensor was mounted on a Fiber Mounting Apparatus with an Invar Base, and glued on the Invar Base through the glue holes. The glue was left for 48 hours at room temperature to dry. At the end, the sensor on Invar Base was sheltered with a protective cover [59].

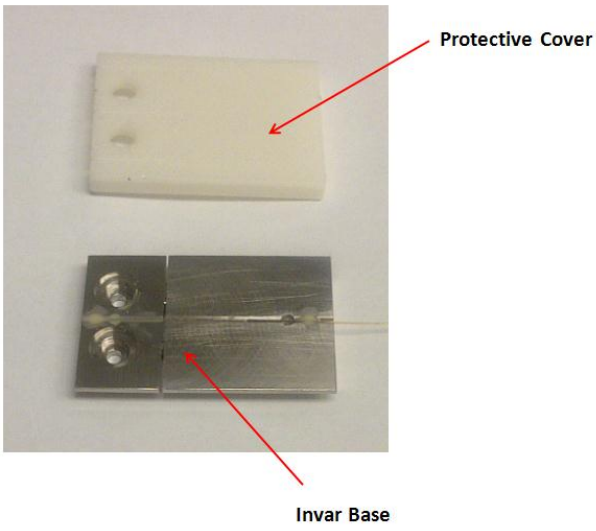

Figure 6-3 Invar base and protective cover

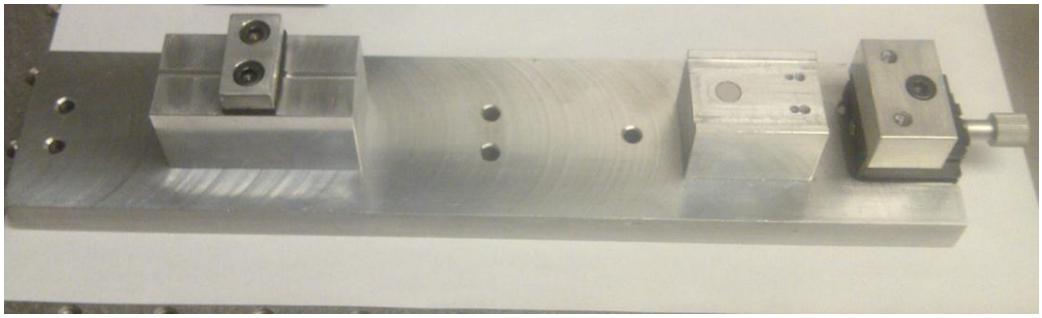

Figure 6-4 Fiber mounting apparatus

6.1.3 Calibration procedure

After the sensor was connected to the interrogator and the equipment (a heater or a motion controller) was turned on, we could monitor temperature, force and displacement by FBG sensor [59]. Figure 6-5 shows the calibration workstation and some equipment for testing process.

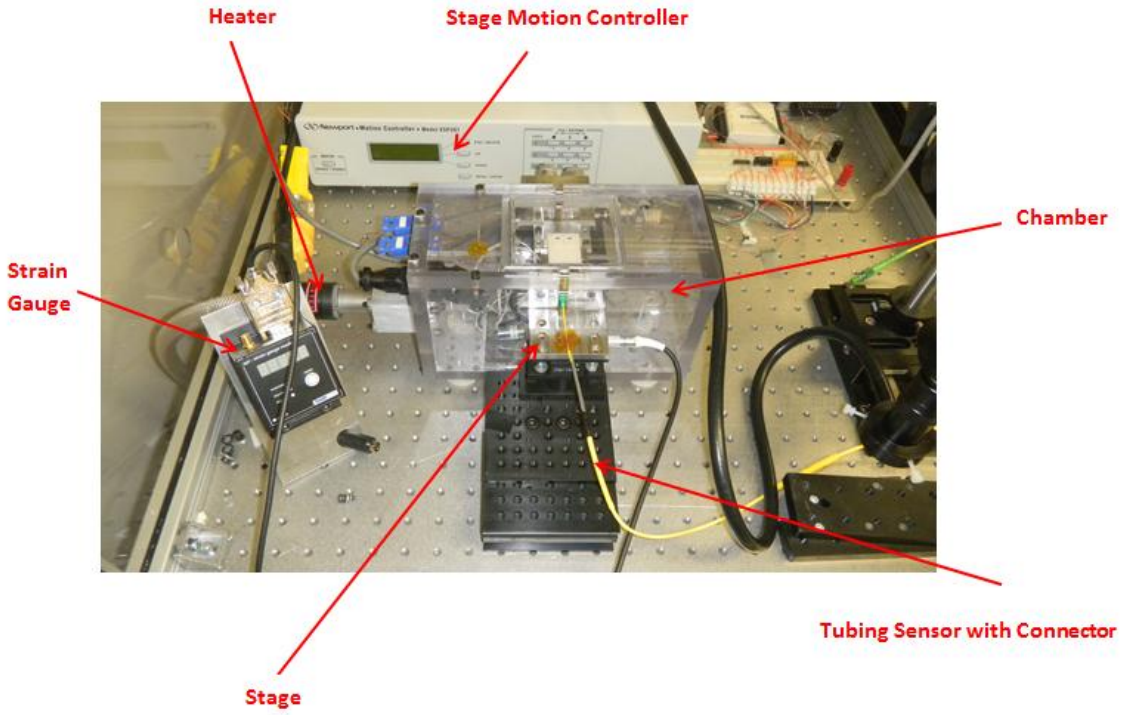

Figure 6-5 The calibration system and testing workstation

6.2 Experimental sensing results

The interrogator was used to detect the signal from the coated FBG sensor. The shift of peak wavelength is used to obtain the sensitivity. The sensing process is reliable and repeatable. The sensor performance was checked several times with no significant deviation during multiple experiments.

6.2.1 Thermal sensing

The thermal sensing was processed on the hot plate and the temperature was controlled by both hot plate and temperature sensing device. Table 6-1 shows the function of temperature and peak wavelength. From the shift of peak wavelength, the thermal sensitivity can be obtained.

Table 6-1 Temperature vs. Peak Wavelength

Temperature (℃)	Peak Wavelength (nm)
25	1549.40±0.01
35	1549.59±0.02
45	1549.82±0.01
55	1550.03±0.02
65	1550.26±0.05
75	1550.47±0.05
85	1550.69±0.05
95	1550.93±0.05
105	1551.18±0.05

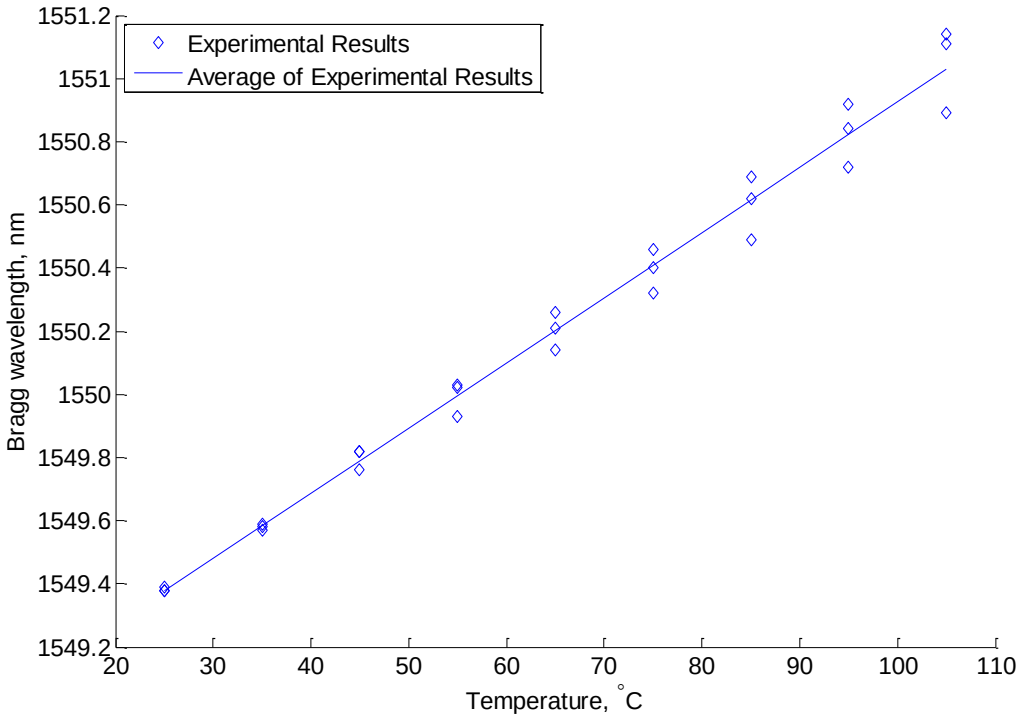

Figure 6-6 Bragg wavelength as a function of temperature for coated FBG

Figure 6-6 shows that the peak wavelength has increased from 1549.4 nm to 1551.18 nm. The rate of increase, which is also called the thermal sensitivity, is approximately 0.0207 ± 0.00211nm/°C. Compared with the original bare sensor's rate of increase, which is 0.01nm/ ℃, it has increased twofold.

The experiments were repeated multiple times to ensure data's repeatability and reliability. There are three times experimental results have been shown in this figure. The straight line described the average of experimental results – 0.0207 ± 0.00211nm/ ℃. The precision reported above is the data deviations through multiple sensitivity measurements. This value is in excellent agreement with the theoretical value (i.e. 0.0229 nm/ ℃).

6.2.2 Force sensing

Several experiments were performed to test the force sensitivity, and the results are shown in Figure 6-7.

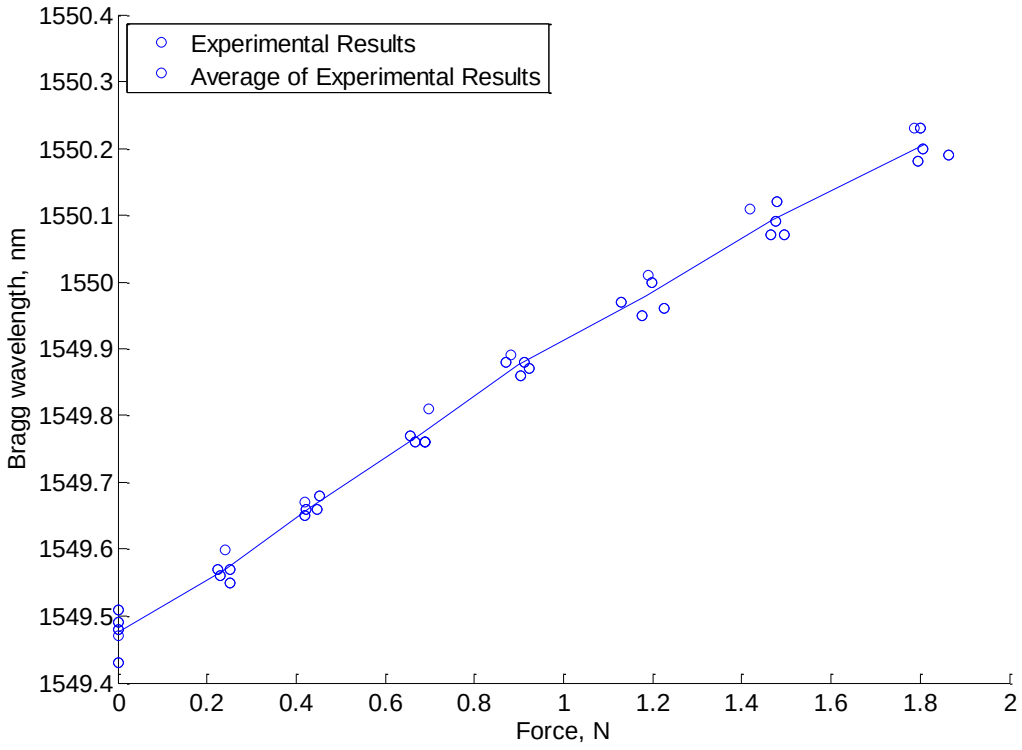

Figure 6-7 Bragg wavelength as a function of force for coated FBG

As seen in Figure 6-7, the peak wavelength is increased from 1549.49 nm to 1550.21 nm. The rate of the increase is 0.4149±0.0218 nm/N approximately. With respect to the original bare sensor's increase rate, which is 1.351 nm/N, the sensor's force sensitivity with 1 μm Ag and 33 μm Ni bi-material coating has been decreased three times.

The experiments were repeated several times to ensure the repeatability and reliability of data. There are five times experimental results of force have been shown. The connection line described the average results, which is 0.4149±0.0218 nm/N. Although reasonably close, this value is still higher than the value obtained from the model which is 0.3035 nm/N. We have figured out that the force sensitivity did not fall as low as the theoretical value. The reason could

be the effect of the thin conductive Ag layer. However, in the theoretical result, for simplicity, the Ag layer was not considered.

6.3 Comparisons and discussion

A process combining LAMM and electroless plating was developed to coat FBGs to not only surround the sensor with a protective layer, but also control the FBG sensor's sensitivity. In this study through many experimental trials conducted, the combined coating process with the reported parameters has been proved with repeatable outcomes in terms of geometrical and physical properties of the coatings and the sensor performance as seen in Figure 6-6 and Figure 6-7. In Chapter 5, although Figure 5-5 shows that the laser sintering process caused some cracks and pores on Ag, however, the Ni layer is still even and smooth with high contents of Ni. Both Table 5-1 and Table 5-2 have shown the high contents of Ni elements from EDAX process. Moreover, this sintering process will remain as an open topic to synthesis crack-free coatings with higher durability resulting in sensors with longer life span.

The experimental results showed that the Ni-Ag layer has increased the thermal sensitivity as twice as the bare FBG and also has provided protection to the sensor at transient high temperature conditions. This raise of sensitivity will improve the accuracy of the sensor to measure temperature variations in many sorts of environments. Figure 6-8 compares the original bare FBG sensitivity with theoretical data and experimental data from room temperature 25℃ to 105℃. As seen in Figure 6-8, the thermal sensitivity of the improved FBG sensor is approximately 0.0207 ± 0.00211nm/℃, almost 2.1 times higher than the bare FBG sensor's thermal sensitivity (0.01 nm/℃). When compared with the theoretical result of 0.0229 nm/℃, there is a slight difference of 4.4% between the modeling and experimental data. This 4.4%

difference can be caused by the model simplification with ignoring the conductive Ag layer and also may be the experimental errors in temperature measurements.

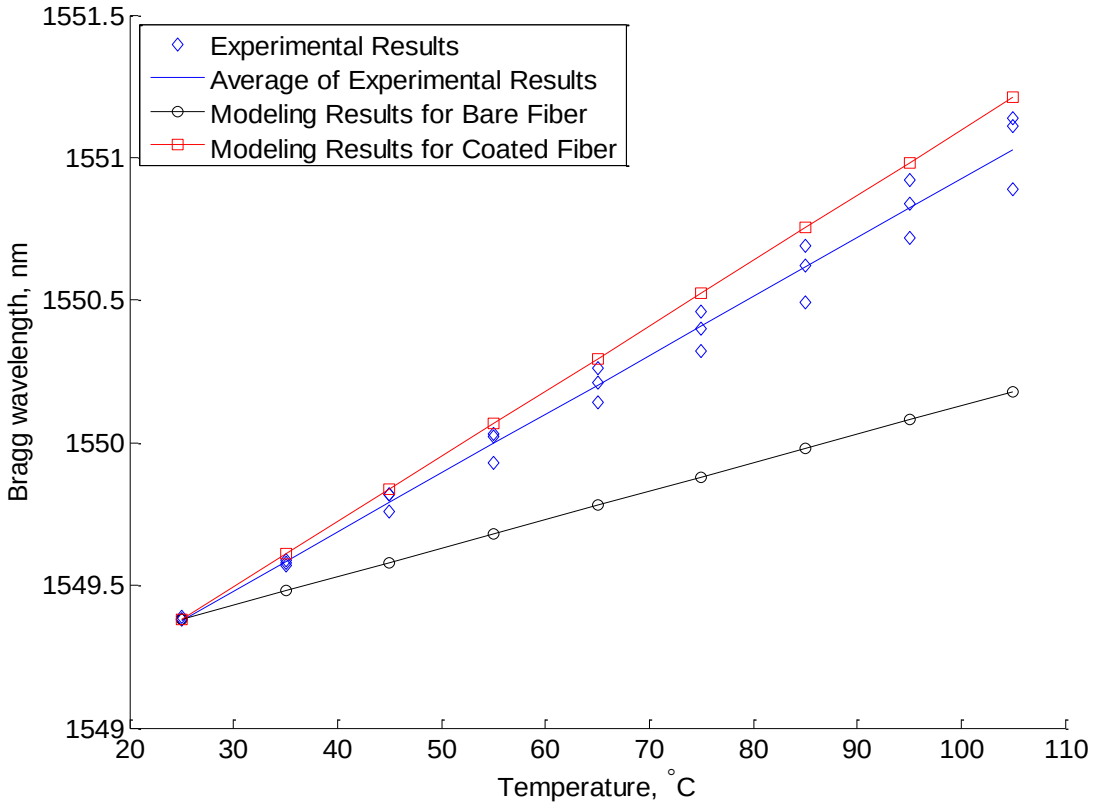

Figure 6-8 Bragg wavelength as a function of temperature for coated and bare FBG

Figure 6-9 shows the data when an axial force in the range of 0 to 1.8 N is applied on the sensor. Except for the experimental data, the modeling results for bare and coated sensor have also been presented in the figure.

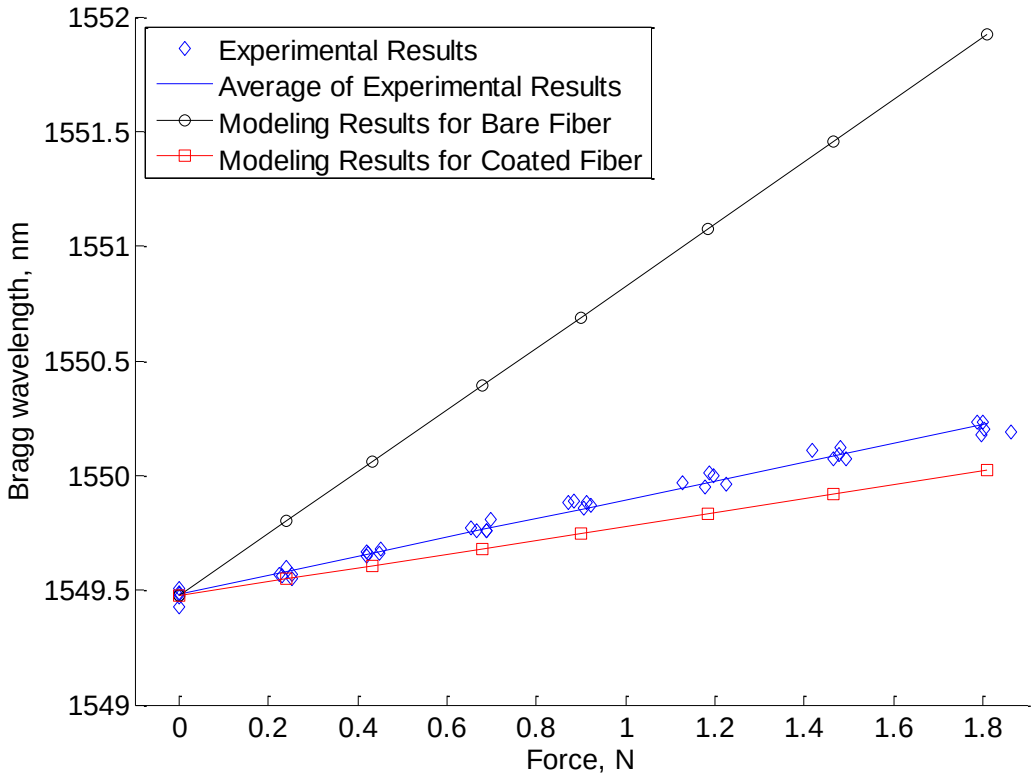

Figure 6-9 Bragg wavelength as a function of force for coated and bare FBG

As seen in the figure, the force sensitivity of coated FBG with 1 μm Ag and 33 μm Ni coating has been decreased to 0.4149nm/N. Compared with that of the original bare sensor, which is 1.351 nm/N, it has been decreased 3 times. However, with respect to the value obtained from the model with coatings which is 0.3035 nm/N, the value is still higher.

The reason may be attributed to the fact that in the opto-mechanical modeling the Ag layer was not considered due to its small thickness, and also to the test setup and uncertainties arising from the friction in the moving parts of motion controlling equipment.

The method in this study provided more convenience, better flexibility and higher thermal sensitivity of FBGs compared to the available studies in literature.

Feng et al. [34] developed an FBG sensor with Cu-Ni coating which showed temperature sensitivity approximately 2 times higher than that of the original FBG. Zhu et al. [67] reported on Ni coated FBGs, with the thickness of 2.8 μm, and the temperature sensitivity of this advanced FBG was 1.3 times higher than the bare FBGs. Zhou et al. [68] presented a single FBG sensor, in which half of the FBG was corroded by hydrofluoric acid, and the other half retained the original cladding. The new developed FBG sensor could show different force sensitivity from two grating halves because of the different cross-section areas. However, in their experiment, the sensor could retain its thermal sensitivity at 9.7 pm/℃, and force sensitivity was shown as 0.784 nm/N. Li et al. [69] used chemical plating and electroplating to plate Ni on the FBG sensor partially. The part of FBG with metallic coating showed higher thermal sensitivity which had increased more than twice than the non-metallized FBG part's original sensitivity. Also, the force sensitivity remained 0.082 nm/N.

After comparing with other results reported in the literature, the method in this thesis provides comparable and higher thermal sensitivity which is adjustable by controlling the geometry of sensor's bi-material coatings. This methodology has resulted in lower force sensitivity; however, the bi-material coating thickness parameters were selected in a way to result in a minimum reduction in force sensitivity and optimum enhancement in thermal sensitivity.

6.4 Summary

The experimental results have been reported in this chapter. With respect to the original data and the theoretical data, the thermal sensitivity obtained from the experiments has been increased twice than the original sensitivity and is also close to the theoretical data. The slight

difference between them is acceptable. The force sensitivity has been decreased significantly when compared with the original one. However, the experimental result still showed higher force sensitivity than the theoretical result. The reason could be the Ag conductive layer which has been ignored in the theoretical model, because in the analytical model above, even thin Ag layer could increase the thermal sensitivity or decrease the force sensitivity.

Chapter 7

Conclusions and Future work

7.1 Conclusion

The following conclusions can be drawn from this thesis:

1. An advanced coating process including LAMM and electroless plating has been developed to firstly deposit a thin conductive silver layer on the optical FBG sensor and to secondly coat a thicker Ni layer right on the Ag conductive layer for both high temperature protection and thermal sensitivity enhancement.
2. A high thermal sensitivity optical FBG sensor with bi-material coating, which can be embedded into a smart tool, has been developed in this thesis.
3. In this study, different kinds of coating materials were analyzed by an opto-mechanical model, and the optimum material and thickness were selected on the basis of the results of this model and manufacturability. Based on both the analytical model and the experiments, the bi-material layer was selected with a thickness of 33 μm Ni on a 1 μm thick Ag.
4. During the LAMM process, in order to find the optimum Erbium continuous beam fiber laser power for sintering, laser power was adjusted to three different levels, low-2.5W, medium-3.5W and high-4.5W. In order to enhance agglomeration of nanoparticles and test the effect of the physical high temperature sintering, only the medium power laser sintering process was employed followed by half an hour hot plate sintering at 230℃. The result showed that the low-power produces a better silver surface quality; however, after the Ni electroless plating the medium-power

followed with physical high temperature sintering showed highest content of Ni element among those three samples. It shows that the Ni surface on the conductive layer could be plated more effectively if we could control the high temperature hot plate sintering process properly.

5. A chemical and physical combined activation process was proposed for the electroless plating process. Both 5% $PdCl_2$ solution and steel were applied in this activation process. The potential barrier for Ni deposition was decreased due to which a smooth Ni layer was deposited on the conductive Ag layer successfully.
6. The thermal sensitivity of the coated FBG with 1 μm Ag and 33 μm Ni coating is 0.0207±0.00211nm/℃ approximately, which is almost 2.1 times higher than the original bare FBG's thermal sensitivity. With respect to the theoretical result which is 0.0229nm/℃, the slight difference of 4.4% is acceptable. The force sensitivity in the improved FBG sensor has been decreased to 0.4149nm/N, while the original bare FBG's is 1.351nm/N. The improved FBG's force sensitivity has been decreased almost 3 times along with getting a higher thermal sensitivity. However, when compared with the theoretical result 0.3035nm/℃ from the analytical model, the value of the improved sensor is still higher.

7.2 Future work

In recent years, the application of optical FBG sensors for structural health monitoring has been increasing rapidly. With improved optical sensors, multiple parameters of the structures can be predicted, not only on the surface but inside as well. This thesis is focused on enhancing FBG's sensitivity, however, based on this thesis, there are some works that can be researched in future.

1. In this thesis, the thickness of Ni coating is 33μm that is an optimum thickness for temperature. Based on the model result in Chapter 3, the coating thickness can be decreased to 20μm or less to obtain higher force sensitivity.
2. Based on the theoretical result, price and feasibility, Ni has been selected as sensitivity enhancement material in this thesis. However, if we ignore price and limitation of equipment, material such as gold and silver are also good choices. As model analytical results talked above, to obtain higher sensitivity, Ag and Au require thinner coating. For example, when Ag coating is 20μm, thermal sensitivity is approximately 0.025nm/℃, and the force sensitivity is almost two times higher than 20μm Ni coating.
3. Superstructure FBGs can replace FBG in the thesis to increase its sensitivity. SFBGs have longer period gratings than regular FBGs, and SFBGs can be applied for multi-parameter sensing.
4. FBG sensor in this thesis has been focused on sensing temperature and force. If we can develop other models to predict different structural parameters (such as displacement, strain and humidity), then selecting optimum material and thickness, advanced sensors can be obtained in the end. These advanced sensors can be used for different sensing purposes.

Appendix

Maple code for solving thermal sensitivity and force sensitivity of 33 μm Ni coating FBG sensor

```
restart;

a := 62.5e-6; E1 := 75e9; E2 := 200e9; ν1 := 0.17; ν2 := 0.31; α1
    := 0.55e-6; α2 := 13.4e-6; b := 95.5e-6; t := b - a;
```

$$a := 0.0000625$$

$$E_1 := 7.5\,10^{10}$$

$$E_2 := 2.00\,10^{11}$$

$$\nu_1 := 0.17$$

$$\nu_2 := 0.31$$

$$\alpha_1 := 5.5\,10^{-7}$$

$$\alpha_2 := 0.0000134$$

$$b := 0.0000955$$

$$t := 0.0000330$$

```
Areaf := π·a^2;
```

$$Areaf := 3.90625\,10^{-9}\,\pi$$

```
Areac := π·(b^2 - a^2);
```

$$5.21400\,10^{-9}\,\pi$$

$$3.14\,b^2 - 1.22656250\,10^{-8}$$

$$\sigma_{rr1} := \frac{-alpha_1 \cdot E_1 \cdot dT}{2 \cdot \left(1 - \nu_1\right)} + C_{11};$$

$$-24849.39759\,dT + C_{11}$$

$$\sigma_{rr2} := \frac{-alpha_2 \cdot E_2 \cdot dT}{2 \cdot \left(1 - \nu_2\right)} + C_{12} \cdot \left(1 - \frac{a^2}{r^2}\right) + \frac{C_{22}}{r^2}$$

$$-1.942028986\,10^{6}\,dT + C_{12}\left(1 - \frac{3.90625\,10^{-9}}{r^2}\right) + \frac{C_{22}}{r^2}$$

$$\sigma_{\theta 1} := 2 \cdot C_{11} - \sigma_{rr1} - \frac{\alpha_1 \cdot E_1 \cdot dT}{1 - \nu_1}$$

$$-24849.39759\, dT + C_{11}$$

$$\sigma_{\theta 2} := \left(2 \cdot C_{12} - \sigma_{rr2} - \frac{\alpha_2 \cdot E_2 \cdot dT}{1 - \nu_2} \right)$$

$$2\, C_{12} - 1.942028985\, 10^{6}\, dT - C_{12} \left(1 - \frac{3.90625\, 10^{-9}}{r^2} \right) - \frac{C_{22}}{r^2}$$

$$\varepsilon_{zz1} := \frac{1}{E_1} \left(\sigma_{zz1} - \nu_1 \cdot \left(\sigma_{rr1} + \sigma_{\theta 1} \right) \right) + \alpha_1 \cdot dT$$

$$1.333333333\, 10^{-11}\, \sigma_{zz1} + 6.626506024\, 10^{-7}\, dT - 4.533333332\, 10^{-12}\, C_{11}$$

$$\varepsilon_{zz2} := \frac{1}{E_2} \left(\sigma_{zz2} - \nu_2 \cdot \left(\sigma_{rr2} + \sigma_{\theta 2} \right) \right) + \alpha_2 \cdot dT$$

$$5.000000000\, 10^{-12}\, \sigma_{zz2} + 0.00001942028986\, dT - 3.100000000\, 10^{-12}\, C_{12}$$

$$eq1 := simplify\left(\varepsilon_{zz1} = \varepsilon_{zz2} \right)$$

$$1.333333333\, 10^{-11}\, \sigma_{zz1} + 6.626506024\, 10^{-7}\, dT - 4.533333332\, 10^{-12}\, C_{11} = 5.000000000\, 10^{-12}\, \sigma_{zz2} + 0.00001942028986\, dT - 3.100000000\, 10^{-12}\, C_{12}$$

$$eq2 := int\left(\sigma_{zz1} \cdot 2 \cdot \pi \cdot r, r = 0 \,..\, a \right) + int\left(\sigma_{zz2} \cdot 2 \cdot \pi \cdot r, r = a \,..\, b \right) = F$$

$$1.227184630\, 10^{-8}\, \sigma_{zz1} + 1.638026410\, 10^{-8}\, \sigma_{zz2} = F$$

$$eq3 := eval\left(\sigma_{rr2}, r = b \right) = 0$$

$$-1.942028986\, 10^{6}\, dT + 0.5716948547\, C_{12} + 1.096461172\, 10^{8}\, C_{22} = 0$$

$$\varepsilon_{rr1} := simplify\left(\frac{1}{E_1} \left(\sigma_{rr1} - \nu_1 \cdot \left(\sigma_{zz1} + \sigma_{\theta 1} \right) \right) + \alpha_1 \cdot dT \right)$$

$$2.750000001\, 10^{-7}\, dT + 1.106666666\, 10^{-11}\, C_{11} - 2.266666666\, 10^{-12}\, \sigma_{zz1}$$

$$\varepsilon_{rr2} := simplify\left(\frac{1}{E_2} \left(\sigma_{rr2} - \nu_2 \cdot \left(\sigma_{zz2} + \sigma_{\theta 2} \right) \right) + \alpha_2 \cdot dT \right)$$

$$\frac{1}{r^2}\left(1.953125000\,10^{-22}\left(3.430399997\,10^{16}\,dT\,r^2 + 1.766400000\,10^{10}\,C_{12}\,r^2 - 131.\,C_{12} + 3.353600000\,10^{10}\,C_{22} - 7.936000000\,10^{9}\,\sigma_{zz2}\,r^2\right)\right)$$

$$\varepsilon_{\theta 1} := simplify\left(\frac{1}{E_1}\cdot\left(\sigma_{\theta 1} - \nu_1\cdot\left(\sigma_{rr1} + \sigma_{zz1}\right)\right) + \alpha_1\cdot dT\right)$$

$$\varepsilon_{\theta 1} := 2.750000001\,10^{-7}\,dT + 1.106666666\,10^{-11}\,C_{11} - 2.266666666\,10^{-12}\,\sigma_{zz1}$$

$$\varepsilon_{\theta 2} := simplify\left(\frac{1}{E_2}\cdot\left(\sigma_{\theta 2} - \nu_2\cdot\left(\sigma_{rr2} + \sigma_{zz2}\right)\right) + \alpha_2\cdot dT\right)$$

$$\varepsilon_{\theta 2} := \frac{1}{r^2}\left(1.953125000\,10^{-22}\left(1.766400000\,10^{10}\,C_{12}\,r^2 + 3.430400003\,10^{16}\,dT\,r^2 + 131.\,C_{12} - 3.353600000\,10^{10}\,C_{22} - 7.936000000\,10^{9}\,\sigma_{zz2}\,r^2\right)\right)$$

$$u1 := int\left(\varepsilon_{rr1}, r = 0\,..r\right)$$

$$u1 := 2.750000001\,10^{-7}\,dT\,r + 1.106666666\,10^{-11}\,C_{11}\,r - 2.266666666\,10^{-12}\,\sigma_{zz1}\,r$$

$$u2 := int\left(\varepsilon_{rr1}, r = 0\,..a\right) + int\left(\varepsilon_{rr2}, r = a\,..r\right) \text{ assuming } r > 0 \textbf{ and } a > 0$$

$$v1 := int\left(r\cdot\varepsilon_{\theta 1} - u1, \theta = 0\,..\theta\right)$$

$$v1 := r\left(2.750000001\,10^{-7}\,dT + 1.106666666\,10^{-11}\,C_{11} - 2.266666666\,10^{-12}\,\sigma_{zz1}\right)\theta - 2.750000001\,10^{-7}\,dT\,r\,\theta - 1.106666666\,10^{-11}\,C_{11}\,r\,\theta + 2.266666666\,10^{-12}\,\sigma_{zz1}\,r\,\theta$$

$$v2 := int\left(r\cdot\varepsilon_{\theta 2} - u2, \theta = 0\,..\theta\right)$$

$$v2 := \frac{1}{r}\left(1.953125000\,10^{-22}\left(1.766400000\,10^{10}\,C_{12}\,r^2 + 3.430400003\,10^{16}\,dT\,r^2 + 131.\,C_{12} - 3.353600000\,10^{10}\,C_{22} - 7.936000000\,10^{9}\,\sigma_{zz2}\,r^2\right)\theta\right) - 1.\,u2\,\theta$$

$$eq4 := \left(int\left(\sigma_{\theta 2}, r = a..\ b\right)\right) + int\left(\sigma_{\theta 1}, r = 0\,..a\right) = 0 \text{ assuming } b > 0 \textbf{ and } a > 0$$

$$-65.64004385\,dT - 5528.795812\,C_{22} + 0.00005459685864\,C_{12} + 0.00006250000000\,C_{11} = 0$$

$$-65.64004385\,dT - 5528.795812\,C_{22} + 0.00005459685864\,C_{12} + 0.00006250000000\,C_{11} = 0$$

$eq5 := simplify((eval(v1, r = a) = eval(v2, r = a)))$

$$eq5 := -3.750000000\,10^{-21}\,dT\theta + 5.000000000\,10^{-26}\,C_{11}\,\theta - 2.500000000\,10^{-26}\,\sigma_{zz1}\,\theta = 6.250000000\,10^{-16}\,\theta\,C_{12} + 4.187500003\,10^{-10}\,dT\theta - 1.048000000\,10^{-7}\,\theta\,C_{22} - 9.687500000\,10^{-17}\,\theta\,\sigma_{zz2} - 1.\,u2\,\theta$$

$eq6 := simplify\left(\left(eval\left(\varepsilon_{\theta 1}, r = a\right) = eval\left(\varepsilon_{\theta 2}, r = a\right)\right)\right)$

$$eq6 := 2.750000001\,10^{-7}\,dT + 1.106666666\,10^{-11}\,C_{11} - 2.266666666\,10^{-12}\,\sigma_{zz1} = 1.000000000\,10^{-11}\,C_{12} + 0.000006700000006\,dT - 0.001676800000\,C_{22} - 1.550000000\,10^{-12}\,\sigma_{zz2}$$

$$A := \left(\frac{1}{2}\left(\text{sqrt}\left(\left(\sigma_{zz2} - \sigma_{rr2}\right)^2 + \left(\sigma_{zz2} - \sigma_{\theta 2}\right)^2 + \left(\sigma_{\theta 2} - \sigma_{rr2}\right)^2\right)\right)\right):$$

$Res := simplify\left(solve\left(\{eq1, eq2, eq3, eq4, eq6\}, \left[C_{11}, C_{12}, C_{22}, \sigma_{zz1}, \sigma_{zz2}\right]\right)\right) assuming\, b > 0:$

$assign(Res[1,1]) : C_{11} := Res[1,1] : assign(Res[1,2]) : C_{12} := Res[1,2] : assign(Res[1,3]) : C_{22} := Res[1,3] : assign(Res[1,4]) : \sigma_{zz1} := Res[1,4] : assign(Res[1,5]) : \sigma_{zz2} := Res[1,5]:$

$simplify\left(\varepsilon_{rr1}\right);$

$$0.000005447792915\,dT - 0.00005478827427\,F = 0.000005447792915\,dT - 0.00005478827427\,F$$

$Res[1,1]$

$$\left(6.749729255\,10^{5}\,dT - 1.405733814\,10^{6}\,F = 6.749729255\,10^{5}\,dT - 1.405733814\,10^{6}\,F\right) = 6.749729255\,10^{5}\,dT - 1.405733814\,10^{6}\,F$$

$r := 0;$

$$r := 0$$

$simplify(\varepsilon_{zz1})$

$$0.00001111399367\,dT + 0.0002371461114\,F = 0.00001111399367\,dT + 0.0002371461114\,F$$

$simplify(\varepsilon_{rr1})$

$$0.000005447792915\,dT - 0.00005478827427\,F = 0.000005447792915\,dT - 0.00005478827427\,F$$

$simplify(\sigma_{zz2})$

$$-7.591801551\,10^{5}\,dT + 4.808217808\,10^{7}\,F = -7.591801551\,10^{5}\,dT + 4.808217808\,10^{7}\,F$$

$\varepsilon_{zz1} := 0.00001111399367\,dT + 0.0002371461114\,F$

$$\varepsilon_{zz1} := 0.00001111399367\,dT + 0.0002371461114\,F$$

$\varepsilon_{rr1} := 0.000005447792915\,dT - 0.00005478827427\,F$

$$\varepsilon_{rr1} := 0.000005447792915\,dT - 0.00005478827427\,F$$

$p_{11} := 0.113; p_{12} := 0.252; dn := 1.2e{-}5; \Lambda := 5.37e{-}7; \alpha_1 := 5.5e{-}7; n_{eff} := 1.44405;$

$$p_{11} := 0.113$$

$$p_{12} := 0.252$$

$$dn := 0.000012$$

$$\Lambda := 5.37\,10^{-7}$$

$$\alpha_1 := 5.5\,10^{-7}$$

$$n_{eff} := 1.44405$$

$$\Delta\lambda_B := \varepsilon_{zz1}\cdot 2\,\Lambda\cdot n_{eff} - \frac{(p_{11}+p_{12})\varepsilon_{rr1}\cdot n_{eff}^{\,2} + p_{12}\varepsilon_{zz1}\cdot n_{eff}^{\,2}}{2}\cdot 2\,\Lambda\cdot n_{eff} + \frac{1}{n_{eff}}\cdot dn\cdot dT\cdot 2\,\Lambda\cdot n_{eff} + \frac{n_{eff}^{\,2}}{2}(p_{11}+2p_{12})\alpha_1\cdot dT\cdot 2\,\Lambda\cdot n_{eff}$$

$$\Delta\lambda_B := 2.292925877\,10^{-11}\,dT + 3.034936494\,10^{-10}\,F$$

$$simplify(\Delta\lambda_B)$$

$$2.292925877\,10^{-11}\,dT + 3.034936494\,10^{-10}\,F$$

$$\Delta\lambda_B := (F, dT) \to 2.292925877\,10^{-11}\,dT + 3.034936494\,10^{-10}\,F$$

$$\Delta\lambda_B := (F, dT) \to \frac{2.292925877\,dT}{100000000000} + \frac{3.034936494\,F}{10000000000}$$

This code was developed by Dr. Hamidreza Alemohammad and Xixi Zhang.

References

[1] Jackson, D. A., Overview of fiber sensor developments, in the edited book of "Optical Fiber Sensor Technology ,1st ed. London: Chapman & Hall, 1995" Edited by Grattan, K. T. V. and Meggitt, B. T.,

[2] Yu, F. T.S. and Yin, S., ″Fiber optic sensors,″ 1st ed. New York: Marcel Dekker, 2002

[3] Dawood, T. A., Shenoi, R. A. and Sahin, M., "A procedure to embed fibre Bragg grating strain sensors into GFRP sandwich structures," Composites Part A: Applied Science and Manufacturing, vol: 38-1, pp:217-226, 2007

[4] Ling, H. Y., Lau, K. T., Cheng, L. and Jin, W. "Utilization of embedded optical fiber sensors for delamination characterization in composite laminates using a static strain method," Smart Materials and Structures, vol:14, pp: 1377-1386, 2005

[5] Lau, K. T., Chan, C. C., Zhou, L. M. and Jin, W. "Strain monitoring in composite-strengthened concrete structures optical fibre sensors," Composites Part B: Engineering, vol: 32, pp: 33-45, 2001

[6] Kashyap, R., Fiber Bragg Gratings, 1st ed. San Diego: Academic Press, 1999

[7] Sandlin, S. and Hokkanen, A. "Embedding optical fibers in metal alloys," IEEE Instrumentation and Measurement Magazine, vol: 6-2, pp: 31-36, 2003

[8] Kong, C.Y. and Soar, R.C. "Fabrication of metal-matrix composites and adaptive composites using ultrasonic consolidation process," Materials Science and Engineering A, vol: 412, pp:12-18, 2005

[9] Iadicicco, A., Campopiano, S., Paladino, D., Cutolo, A., Cusano, A., Bock, W. "Gold coated long period gratings in single and multi-layer configuration for sensing applications" Sensors and Microsystems, pp: 133-136, 2009

[10] Kashyap, R., Fiber Bragg Gratings, 2nd ed. Burlington : Academic Press, 2010

[11] Alemohammad, H., Toyserkani, E., Paul, C. P. "Fabrication of smart cutting tools with embedded optical fiber sensors using combined laser solid freeform fabrication and moulding techniques," Optics and Lasers in Engineering, vol: 45-10, pp: 1010-1017, Oct. 2007

[12] Lee, C. E., Alcoz, J. J., Gibler, W. N., Atkins, R. A. and Taylor, H. F. "Method for embedding optical fibers and optical fiber sensors in metal parts and structures," Proceedings of SPIE - The International Society for Optical Engineering, vol: 1588, pp:110-116, 1991

[13] Li, Y. L., Liu, W., Feng, Y. and Zhang, H. "Ultrasonic embedding of nickel-coated fiber Bragg grating in aluminum and associated sensing characteristics," Optical Fiber Technology, vol: 18-1, pp: 7-13, 2012

[14] Alemohammad, H. and Toyserkani, E. "Metal embedded optical fiber sensors: Laser-based layered manufacturing procedures", Journal of Manufacturing Science and Engineering, a Transaction of ASME, vol: 133(3): 031015-1, 12 pages, 2011

[15]Alemohammad, H. and Toyserkani, E. "Superstructure fiber Bragg grating sensors with enhanced sensitivity using laser assisted direct writing of on-fiber thin films," 28th International Congress on Applications of Lasers and Electro-Optics, ICALEO, Orlando, 2009

[16] Yang, M. and Dai, J. "Review on optical fiber sensors with sensitive thin films," Photonic Sensors, vol: 2-1, pp: 14-28, 2012

[17] Maier, R. R. J., MacPherson, W. N., Barton, J. S., Carne, M., Swan, M., Sharma, J. N., Futter, S. K., Knox, D. A., Jones, B. J. S. and McCulloch, S. "Fibre optic strain and configuration

sensing in engineering components produced by additive layer rapid manufacturing," 10th IEEE SENSORS Conference, Limerick,2011

[18] Sandlin, S., Kinnunen, T., Ramo, J., Sillanpaa, M. "A simple method for metal re-coating of optical fibre Bragg gratings" Surface & Coatings Technology, vol: 201, pp: 3061-3065, 2006

[19] Hill K. O., Fiber Bragg gratings, in the edited book of "*Fiber Optics Handbook,* Florida: McGraw-Hill, 2002", edited by Bass, M. and Stryland, E. W. V.

[20] Othonos, A. and Kalli, K. *Fiber Bragg Gratings: Fundamentals and Applications in Telecommunications and Sensing,* 1st ed. Boston: Artech House, 1999

[21] Hill, K. O., Fujii, Y. and Johnson, D. C. "Photosensitivity in Optical Fiber Waveguides: Application to Reflection Filter Fabrication," Applied Physics Letters, vol: 32-10, pp: 647-649, 1978

[22] Kawasaki, B. S., Hill, K. O. and Johnson, D.C. "Narrow-Band Bragg Reflectors in Optical Fibers," Optics Letters, vol:3-8, pp: 66-68, 1978

[23] Meltz, G., Morey, W. W. and Glenn, W. H. "Formation of Bragg gratings in optical fiber by a transverse holographic method," Optics Letter, vol: 14, pp: 823, 1989

[24] Othonos, A. Bragg gratings in optical fibers: fundamentals and applications, in the edited book of "Optical Fiber Sensor Technology Advanced Applications – Bragg Gratings and Distributed Sensors, 1st ed. Netherlands: Kluwer Academic Publishers, 2000", edited by Grattan, K. T. V. and Meggitt, B. T.

[25] Hill, K. O., Malo, B., Bilodeau, F., Johnson, D. C. and Albert, J. "Bragg gratings fabricated in monomode photosensitive optical fiber by UV exposure through a phase-mask" Applied Physics Letters, vol: 62, pp: 1035-7, 1993

[26] Malo, B., Hill, K. O., Bilodeau, F., Johnson, D. C. and Albert, J. "Point-by-point fabrication of micro-Bragg gratings in photosensitive fiber using single excimer pulse refractive index modification techniques" Electronics Letters, vol: 29, pp: 1270-2, 1993

[27] Mihailov, S. and Gower, M. "Recording of efficient high-order Bragg reflectors in optical fibers by mask image projection and single pulse exposure with an excimer laser" Electronics Letters, vol:30, pp: 707-8, 1994

[28] Malo, B., Bilodeau, F., Johnson, D. C., Albert, J. and Hill, K. O. "Single-excimer-pulse writing of fiber gratings by use of a zero-order mulled phase-mask: grating spectral response and visualization of index perturbations" Optics Letter, vol: 18, pp: 1277-9. 1993

[29] Martin, J. and Ouellette, F. "Novel writing technique of long and highly reflective in-fiber gratings" Electronics Letters, vol: 30, pp: 811-2, 1994

[30] Byron, K.C., Sugden, K., Bircheno, T. and Bennion, I. "Fabrication of chirped Bragg gratings in photosensitive fibre" Electronics Letters, vol: 29, pp: 1659-60, 1993

[31] Kashyap, R., McKee, P. F. and Armes, D. "UV written reflection grating structures in photosensitive optical fibres using phase-shifted phase masks" Electronics Letters, vol: 30, pp:1977-8, 1994

[32] "Strain Diagram." Brigham Young University. Web. 17 Dec 2010. <http://www.photonics.byu.edu/fbg.phtml>

[33] Li, X. C., Tang, W. L., Golnas, A. "Embedding and characterization of fiber-optic and thin-film sensors in metallic structures" Sensor Review, vol: 24-4, pp: 370-377, 2004

[34] Feng, Y., Zhang, H., Li, Y. L., Rao, C. F. "Temperature sensing of metal-coated fiber bragg grating" Transactions on mechatronics, vol: 15-4, pp: 511-519, 2010

[35] Mou, C. B., Saffari, P., Li, D., Zhou, K.M., Zhang, L., Soar, R. and Bennion, I. "Smart structure sensors based on embedded fibre Bragg grating arrays in aluminium alloy matrix by ultrasonic consolidation" Measurement Science and Techinology, vol: 20-3, 2009

[36] Lupi, C., Felli, F., Brotzu, A., Caponero, M. A., Paolozzi, A. "Improving FBG sensor sensitivity at cryogenic temperature by metal coating" Sensor Journal, vol:8-7, pp: 1299-1304, 2008

[37] Feng, Y., Zhang, H., Li, Y. L. and Peng, G. "Highly sensitive Ni-Cu duplex metal coated fiber Bragg grating temperature sensor" Symposium on Photonics and Optoelectronics, Wuhan, China, Article number: 5230237, 2009

[38] Lee, C. H., Kim, M. K., Kim, K. T., Lee, J. "Enhanced temperature sensitivity of fiber Bragg grating temperature sensor using thermal expansion of copper tube" Microwave and Optical Technology Letters, vol: 53-7, pp: 1669-1671, 2011

[39] Song, D. C., Zou, J. L., Wei, Z. X., Yang, S.M. and Cui, H. L. "High-sensitivity fiber Bragg grating pressure sensor using metal bellows," Optical Engineering, vol: 48-3, 2009

[40] Metev, S. M. and Veiko, V. P. Laser-assisted Microtechnology, 1st ed. Springer, Verlag Berlin Heidelberg, Germany, 1994

[41] Udd, E. Fiber optic smart structure technology, in the edited book of: “Fiber Optic Smart Structures, John Wiley & Sons Inc., New Jersey, 1995”, edited by Udd, E.

[42] Udd, E. Fiber optic sensor overview, in the edited book of: “Fiber Optic Smart Structures, John Wiley & Sons Inc., New Jersey, 1995”, edited by Udd, E.

[43] Berthold III, J. W., Industrial applications of fiber optic sensors, in the edited book of "Fiber Optic Smart Structures: An Introduction for Engineers and Scientists, Wiley, New York, 1991", edited by Udd, E.

[44] Udd, E., Blom, R. G., Tralli, D., Saaski, E. and Dokka, R. ″Application of the Sagnac Interferometer Based Strain Sensor to an+ Earth Movement Detection System,″ Proc. SPIE-Int. Soc. Opt. Eng., vol: 2191, pp: 126, 1994

[45] Nguyen, A. D. and Rakow, A. S. ″A fiber Bragg grating interrogation system for health monitoring of metals and composites″ The International Society for Optical Engineering, San Diego, CA, vol: 7649, 2010

[46] Suresh, R., Tjin, S. C., Ngo, N. Q., ″Application of a new fiber Bragg grating based shear force sensor for monitoring civil structural components″ Smart Materials and Structures, vol: 14, pp: 982-988,2005

[47] Richter-Trummer, V., Silva, S. O., Peixoto, D. F. C., Frazao, O., Moreira, P. M. G. P., Santos, J. L., Castro, P. M. S. T. ″Fibre Bragg grating sensors for monitoring the metal inert gas and friction stir welding processes″ Measurement Science and Technology, vol: 21, pp: 085105(8pp), 2010

[48] Wu, Y. H., Shao, C. J., Qu, W. J., Zhou, W., Cai, H. W. ″ Study on FBG strain sensor for application to large engineering long term health monitoring,″ Guangdianzi Jiguang/Journal of Optoelectronics Laser, vol: 21- 4, pp: 481-484, 2010

[49] Amano, M., Okabe, Y., Takeda, N., Ozaki, T. ″Structural Health Monitoring of an Advanced Grid Structure with Embedded Fiber Bragg Grating Sensors,″ Structural Health Monitoring, vol:6- 4, pp: 309-324, 2007

[50] Yue, L., Huang, J. and Yang Y. Application of FBG sensors in strengthening and maintenance monitoring of old bridges″ 20th International Conference on Optical Fibre Sensors, Edinburgh, vol: 7503, 2009

[51] Chong, S.Y., Lee, J.R., Yun, C.Y., and Sohn, H. ″Design of copper/carbon-coated fiber Bragg grating acoustic sensor net for integrated health monitoring of nuclear power plant ,″ Nuclear Engineering and Design, vol: 241-5, pp: 1889-1898, 2011

[52] Huang, S., Jin, X., Zhang, J., Chen, Y., Wang, Y., Zhou, Z. and Ni, J. ″An optical fiber hydrophone using equivalent phase shift fiber bragg grating for underwater acoustic measurement,″ Photonic Sensors, vol: 1-3, pp: 289-294, 2011

[53] Alemohammad, H. and Toyserkani, E. "Modeling and analysis of fiber optic bragg grating shape sensors" ASME International Mechanical Engineering Congress and Exposition, IMECE 2007, Seattle, WA, USA, 2007

[54] Kim, K.S., Kollar, L. and Springer, G.S. "A model of embedded fiber optic Fabry-Perot temperature and strain sensors," Journal of Composite Materials, vol: 27-17, pp: 1618-1662, 1993

[55] Kim, K.S., Ismail, Y. and Springer, G.S. "Measurement of strain and temperature with embedded intrinsic Fabry-Perot optical fiber sensors," Journal of Composite Materials, vol: 27-17, pp: 1663-1677, 1993

[56] Alemohammad, H. 2010 Development of optical fiber-based sensing devices using laser microfabrication methods PHD Thesis, University of Waterloo (Waterloo, Ontario, Canada)

[57] Baek, D. C., Park, T. S. and Lee, S. B. "Measurement of mechanical properties of electroplated nickel thin film" Key Eng. Mater. vol: 261, pp: 417–22. 2004

[58] David R. Lide (ed), CRC Handbook of Chemistry and Physics, 84th Edition. CRC Press. Boca Raton, Florida, 2003

[59] Cotton, B. Dual-Parameter Fiber Optic Sensor Manufacturing Process User's Guide, Department of Mechanical and Mechatronics Engineering, University of Waterloo, Aug. 2011

[60] Cauchois, R., Saadaoui, M., Legeleux, J., Malia, T., Dubois-Bonvalot, B., Inal, K. and Fidalgo, J. C. "Wire-Bonding on inkjet-printed silver pads reinforced by electroless plating for the chip on flexible board package" Electronics System Integration Technology Conference, Berlin, 2010

[61] Gian, P. W., Shan, X.C., Liang, Y. N., Lok, B. K., Lu, C. W. and Ooi, B. L. "High aspect pattern formation by integration of micro inkjetting and electroless plating" DTIP of MEMS and MOEMS, pp:162-167, 2008

[62] Nakaso, K., Shimada, M., Okuyama, K. and Deppert, K., "Evaluation of the change in the morphology of gold nanoparticles during sintering" Journal of Aerosol Science, vol. 33, no. 7, pp. 1061-1074, 2002.

[63] Arcidiacono, S., Bieri, N. R., Poulikakos, D. and Grigoropoulos, C. P., "On the coalescence of gold nanoparticles" International Journal of Multiphase Flow, vol. 30, no. 7-8, pp. 979-994, 2004.

[64] The Caswell Plating Manual, Version 9, CASWELL Inc. USA

[65] Electroless Nickel Plating, A Guide, Artistic Plating Company, Inc. Milwaukee, WI 53212

[66] Foroozmehr, E., Alemohammad, H. and Toyserkani, E. "Dual-Parameter Optical Fiber Sensors for Structural Health Monitoring" International Workshop on Fibre and Optical Passive Components, WFOPC, 2011

[67]Z.Q. Zhu, Y.J. Chen, Y.F. Zhang, "The temperature sensitivity of fiber Bragg gratings embedded in an Al 6061 matrix by ultrasonic welding" Journal of Intelligent Material Systems and Structures, vol: 22, pp: 2173-2179, 2011

[68] Zhou, W., Zhao, C. L., Dong, X., Zhang, S., Chan, C.C. and Shum, P. "Simultaneous measurement of force and temperature based on a half corroded FBG" Microwave and Optical Technology Letters, vol: 52-9, pp: 2023-2023, 2010

[69] Li, Y., Feng, Y., Peng, X. and Zhang, H. "Simultaneous measurement of the temperature and force using a steel cantilever soldered with a partially nickel coated in-fibre Bragg grating" Optics Communications, 2012